

Comparative Analysis of Charging Systems for Heavy Duty Applications: A Review of Size, Efficiency, Sustainability, and Economic Viability

I. Gheorghită, ir. S. Qazi*, dr. ir. P. Venugopal**, dr. H. S. Bindra***

*Daily Supervisor, **Assistant Professor, ***External Committee Member

BSc. Thesis Electrical Engineering

University of Twente, Department of Electrical Engineering, Mathematics and Computer Science

June 30, 2023

Abstract—The ever-increasing global efforts of combating the causes and effects of climate change have culminated in 2015 with the legally binding adoption of the Paris Agreement. As a result of this treaty, the electrification of the transport sector has been greatly accelerated to quickly decrease its greenhouse gas (GHG) emissions. Light duty vehicles (LDVs) with fully electric powertrains have become more common, cheaper and with extended ranges. These developments, alongside the electrification of heavy-duty vehicles (HDVs) and the maritime sector result in much higher charging power requirements. The scope of this paper is to analyse state-of-the-art technologies that can be used in the charging systems for heavy duty applications (HDAs). We make a qualitative comparison in terms of size, efficiency, sustainability, and economic viability for the three main categories found in literature: alternating current (AC), direct current (DC), and inductive. The comparison is followed by a case study on DC charging with the primary focus on simulation, where we describe the design, operation, and control of a typical two-stage implementation. The analysis emphasizes the importance of topology choice, power factor correction (PFC), direct-quadrature-zero (DQZ) transformation, and integration of solid-state-transformers (SSTs). We realize the simulation and verification of the circuits in the PLECS software. Finally, the results show that DC charging is the most viable technology for large-scale projects, followed by inductive charging in the automation industry. We propose multilevel conversion and mixed charging infrastructure as possible solutions to the current limitations of charging systems.

Index Terms—direct-quadrature-zero (DQZ) transformation, electric ship, energy efficiency, heavy-duty vehicle (HDV), high-frequency transformers, hysteresis current control, inductive charging, phase shifted full bridge (PSFB), solid-state-transformer (SST)

I. INTRODUCTION

The European Commission defines heavy-duty vehicles (HDVs) as “trucks, buses and coaches” [1], while U.S. Census Bureau, the Federal Highway Administration and the Department of Transportation define them as vehicles with load ranges of more than 26001 pounds (~11.8 tonnes), such as: city transit buses, medium and heavy semi-trucks, tows, cement mixers, refrigerator vans, fire trucks, fuel trucks, and tour buses [2], [3].

The extensive range of vehicles that fall under the definition shows their importance in the sector of transportation. By

2014, the European Commission’s estimates showed that HDVs contribute to approximately 25% of the road transport emissions and to 5% of the total European Union’s (EU’s) emissions [1]. Globally, they represent the second largest category of transportation in terms of greenhouse gasses (GHG) emissions [4]. The emission share of each transport subsector can be observed in Fig. 1. In order to meet the goals of the Paris Agreement, significant decarbonization efforts must be undertaken, which, according to the International Council on Clean Transportation (ICCT), involve the electrification of the HDV fleet by 29% to 81% before the middle of the current century [5].

Global CO₂ Emissions from Transport by Subsector

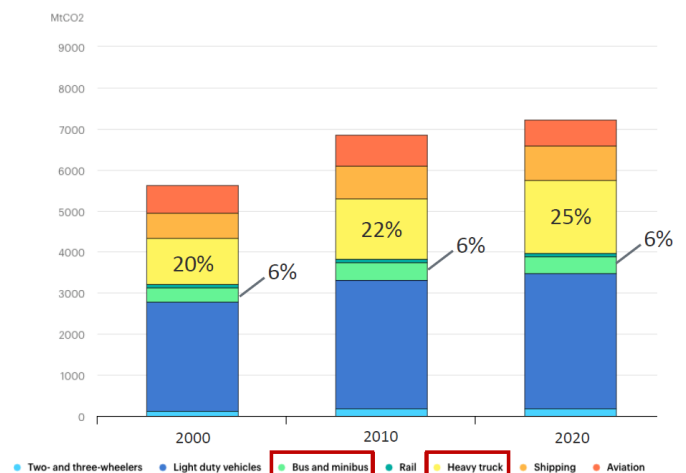


Fig. 1: The contribution of the transport subsectors to global CO₂ emissions [4]

In the context of ever-expanding international trading, the maritime sector has an essential role in the transportation of goods and people. Although it is the most energy-efficient and environmentally friendly method of long-distance travel, its increasing volume is a great cause of concern, as fossil fuels (FFs) are the main source of energy for the ships. Most of the modern vessels still use diesel and gasoline generators to

produce the necessary power, which leads to a large amount of GHG emissions. Their impact can be clearly seen in Fig. 1, where the maritime subsector is the third largest contributor, after LDVs and HDVs, representing approximately 10% of the total emissions. The ships that transport goods over the ocean carry more than 70% of the global volume of cargo and it is expected that they will be responsible for 17% of the carbon emissions by 2050 [6].

However, with the proper initiatives and changes, the ICCT’s research projects that, by 2050, up to 71% of the maritime sector’s emissions could be cut [6]. The zero-emissions technologies, largely represented by fully electric power trains and energy storage, are one of the most important initiatives in that scope.

The electrification of the heavy-duty vehicles and ships cannot be realized in the absence of proper charging infrastructure. The higher energy requirements of these sectors create the need for improvement of the already mature technologies, as well as an incentive to find novel solutions. Research and development of charging technologies advances at the same accelerated pace as the heavy-duty transport sector; therefore, the scope of this paper is to describe and compare the charging systems that appear in recent literature as having the best potential to power the future needs of HDVs and electric ships. The analysis of each technology is based on the data found in the survey and covers four main points of interest: size, efficiency, sustainability, and economic viability. Moreover, the system that is determined as the most viable option becomes the focus of a case study in which its operation is described and simulated. Arguments for suitable topologies and configurations, as well as explanations of the fundamental functional principles are prioritized over detailed component-specific modelling and design.

The structure of the paper is the following: Section II provides more information about the context in which the electrification of the HDV and maritime sectors happens. The main charging technologies are described and compared in Section III. The results of the analysis are summarised and discussed in Section IV and a solution for future charging infrastructure is proposed. In Section V, the requirements and resulting characteristics of the most viable technology are described; the functioning principle, parameter design, and control schemes are explained, followed by the presentation of the simulation results. Those are then discussed in Section VI. Finally, conclusive remarks are given in Section VII, followed by proposals for future research in Section VIII.

II. HEAVY DUTY APPLICATIONS

Before the different charging technologies can be analysed and compared, it is essential to understand the context in which their research and implementation develop. The context in which heavy duty applications (HDAs) are defined is described in the next subsections, as the scope of the charging systems depends on their requirements and nature.

A. Heavy-duty Vehicles Subsector

Although in the previous years both the production and the sales of electric trucks and buses were highly dependent on the amount of subsidies, in 2021 and 2022 the sales increased while the subsidies got progressively smaller. In 2022, approximately 4.5% of the bus sales and 1.2% of truck sales worldwide were electric. In the same year, almost two thirds of the buses purchased in Finland were electric, whereas in the Netherlands and Norway came second, with nearly half of the new buses being electric [7]. Some projections indicate that the market share will rise from the current 10% up to 40% by the year 2025 for e-buses. In the Netherlands, the Ministry of Infrastructure and Water Management signed an agreement with the public transport authorities in 2016, which mandates that all new buses purchased from 2025 onward must be electric and that the entire fleet must be fully electric by the year 2030 [8].

While the electric truck sales remain at a low level, the range of available models keeps expanding and has reached 840 current and announced models [7], which can be found in the database of the Global Drive to Zero Emissions Technology Inventory (ZETI) [9]. The evolution of the number of zero emission vehicles (ZEVs) in the past three years can be seen in Fig. 2. In the Netherlands, the Directorate General for Public Works and Water Management has expressed its intent to replace all the cleaning and freight vehicles with electric vehicles before 2030 [8].

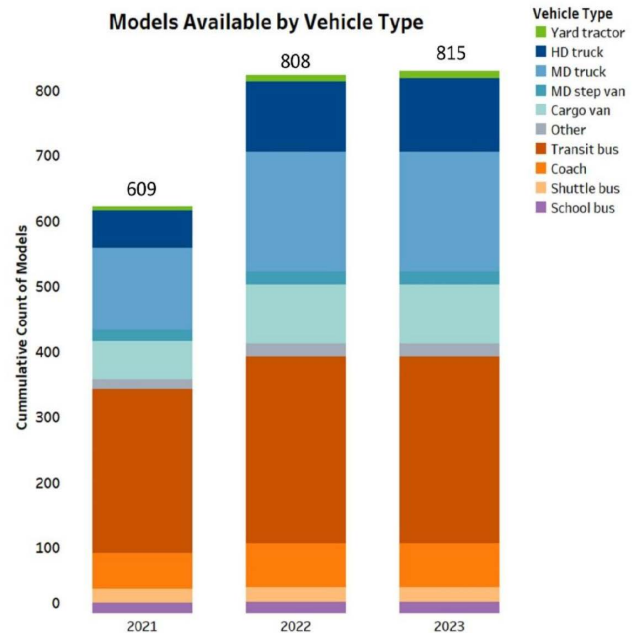


Fig. 2: The number of available and expected ZEV models by vehicle type [10]

One of the biggest concerns regarding the phasing out of internal combustion engine (ICE) vehicles with electric ones is *range anxiety*: the fear that the energy capacity is not sufficient to complete the journey. This is being addressed in the case of light duty vehicles (LDV), where progress is quick compared

to the HDV ranges. For the later, the use scenarios involve much higher energy consumption due to the typical size and weight of the vehicle and its load, while the expansion of the energy storage is limited by the economic viability: it is not profitable to sacrifice the cargo space and weight for oversized batteries. The evolution of the battery capacity of HDV in the period 2019-2022 is presented in [7] and shown in Table I.

TABLE I: Evolution of average range of different HDV types [7]

Vehicle Category	Average Battery Capacity (kWh)				
	2019	2020	2021	2022	Change 2019-2022
Transit bus	264	322	225	345	31%
School bus	155	141	207	137	-0.12%
Shuttle bus	104	119	120	150	0.45%
Coach	316	347	233	266	-0.16%
Cargo van	69	90	57	60	-0.13%
Medium-duty step van	NA	134	155	163	22%*
Medium-duty truck	124	139	99	92	-0.26%
Heavy-duty truck	293	232	372	311	0.06%
Yard tractor	150	184	160	197	31%

*No medium-duty step vans were sold in 2019, so the change is for the 2020-2022 period

Plots depicting the median range of different zero emission bus and truck types in the 2019-2022 period can be seen in Figs. 3 and 4. Although the battery capacity has not increased for all categories, the decrease is less than 1% in all cases, while the increase can be as high as 31%. This is reflected by the general increase in electric bus range that is visible in Fig. 3. While some truck categories have a clear trend of increased range, others show the exact opposite. This can be a result of newer models entering the market that sacrifice the range for other benefits, such as lower costs. Moreover, it is possible that the current range is sufficient for the use cases that the producers and users focus on. As the pool of truck models is still limited, the average is highly volatile and even a small number of new models can drastically change the overall trend [10]. Moreover, the data presented in the plots and table may not be exhaustive and, therefore, it could vary slightly from the real phenomenon.

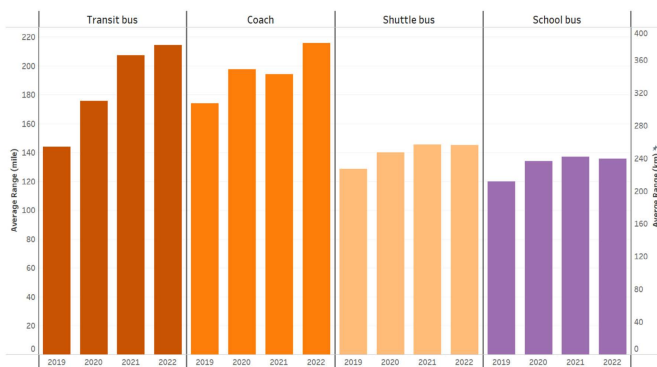


Fig. 3: The evolution of average range of electric buses [10]

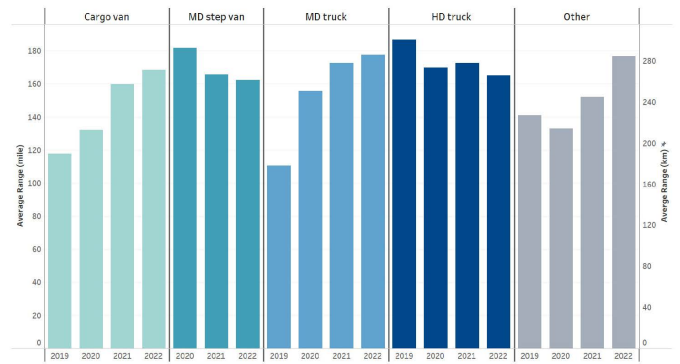


Fig. 4: The evolution of average range of electric trucks [10]

Range anxiety is a problem that pertains to all types of electric vehicles. According to [11], the average usable battery charge of a personal EV is 68 kWh, with some cars going beyond 120 kWh. The nominal values of the batteries in such vehicles are even higher. Scalable battery systems containing one or more 52 kWh and 100 kWh modules are already available for industrial and commercial applications [12]. Drivers of personal EVs want to have a charging experience as short as refuelling an ICE vehicle, while HDV operators require to be able to finish their journeys and work shifts without being interrupted by a recharging break. This leads to fast and super-fast charging technologies to become a priority. In that scope, high power and high voltage charging stations have become more widespread, as well as gaining a more significant role in the current research.

As described by [12], heavy duty applications may use 360 Vdc and 650 Vdc battery modules. Most personal vehicles accept 400 Vdc charging, while there are already models on the market that accept 600 Vdc and even 800 Vdc charging [13]. The required voltage level is expected to rise as to decrease the charging time and to allow higher capacities to be recharged in a feasible manner in all types of applications. The feasible electrification of the powertrain, and the required charging power and voltage levels for HDV are significantly higher than the ones for LDV, as seen in Fig. 5.

B. Maritime Subsector

The current maritime microgrids that represent the ship's electric systems are either AC or DC based, as the loads (such as: propulsion system, refrigeration, heating, navigation system, basic life support) can require either of them. The onshore grid is usually 3-phase AC based, with 50 Hz or 60 Hz frequencies, the former being more prevalent around the world. However, the majority of vessels that have an AC main bus use the latter frequency more often [15].

To reduce the pollution in ports and surrounding areas, the concept of *cold ironing* has been introduced, referring to the transmission of power from shore to berthed ships through an electrical connection, which allows the engines to be shut off. A diagram of an implemented solution of this type is presented in Fig. 6. With the emergence of battery-driven boats and

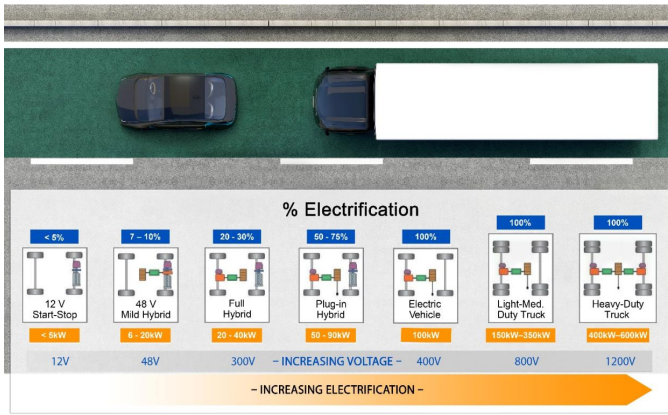


Fig. 5: Charging power and voltage for different powertrain configurations [14]

ships, there is a need to enhance shore-to-ship power delivery systems for onshore charging in addition to cold ironing. In this context, high power charging systems become an essential topic of research, having a similar impact as for the electric HDVs.

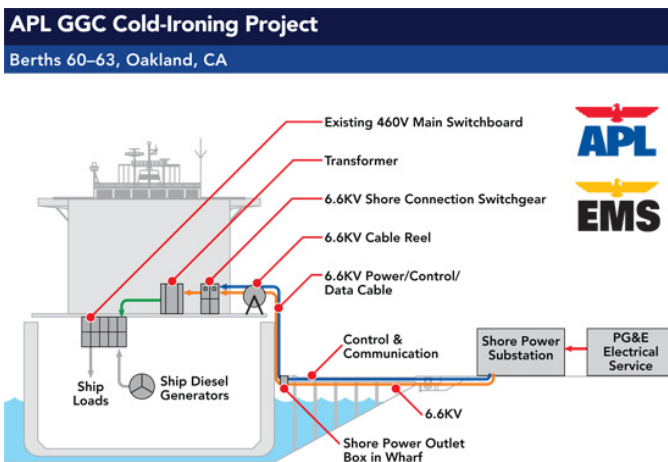


Fig. 6: Cold ironing concept diagram [16]

C. Final Remark

Considering the similar nature and requirements of the powertrains in both the HDV and maritime sector, the heavy duty applications are mostly treated as a whole in the following sections. In the case of subsector-specific (dis)advantages of certain charging systems, the distinction is clearly specified.

III. CHARGING SYSTEMS

There are multiple ways to categorise the existing charging technologies for HDAs. [8] presents three main categories in the hierarchical structure visible in Fig. 7.

Conductive charging refers to the technologies that require a direct, mechanical, and electrical contact with the charging port of the vehicle. They can output either DC or AC and they are grouped in three levels, based on the voltage and power.

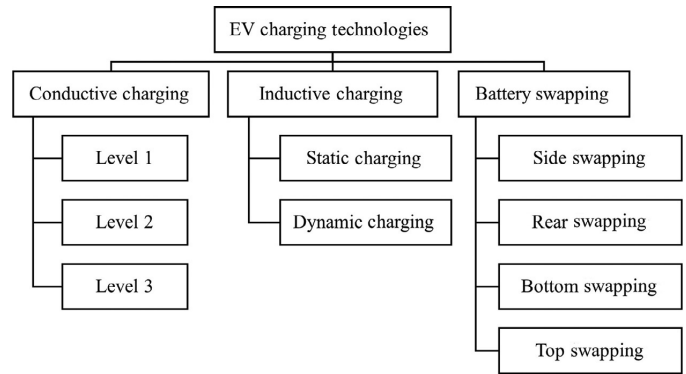


Fig. 7: Categories of charging technologies [8]

The different levels, as defined by the SAE J1772 standard, can be observed in Fig. 8 for both AC and DC [8].

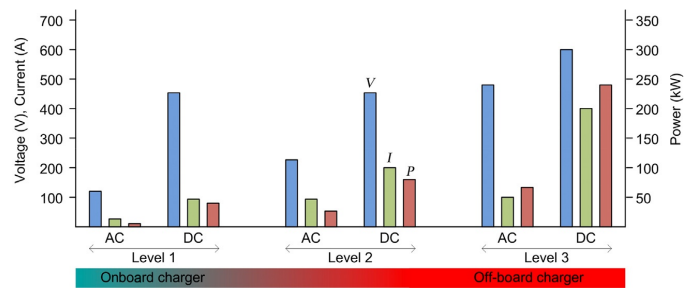


Fig. 8: The voltage (blue), current (green), and power (red) of the different charging levels [8]

Inductive charging requires no direct contact, being also referred to as wireless charging. It is further categorised based on whether the vehicle is moving or not during the charging operation. Finally, the battery swapping technologies include the systems required to make the swapping the vehicle's drained batteries with full ones as quick and safe as possible. As the final category does not directly involve chargers, the following subsections will only focus on AC, DC, and inductive charging.

A. AC Charging

AC charging technology is a direct extension of the electrical grid, which is predominantly AC. However, the batteries in LDVs and HDVs require DC, which makes a conversion stage mandatory. The main purpose of external AC chargers is to properly connect the vehicle to the grid, while the voltage level and current type conversion is realised inside the car, by the on-board charger. This makes the charging a simple operation for the user, especially as it involves almost no additional circuitry to create a charging station [8]. However, the on-board chargers have limited power levels because of the constraints imposed by the connecting cable and the available space for the charging circuit. Therefore, only two levels are typical for AC charging, as portrayed in Fig. 9. The time shown is the necessary period to charge a 60kWh battery [17]. Unfortunately, the available AC power levels are too low to be useful in HDAs, as the charging times would be too long.

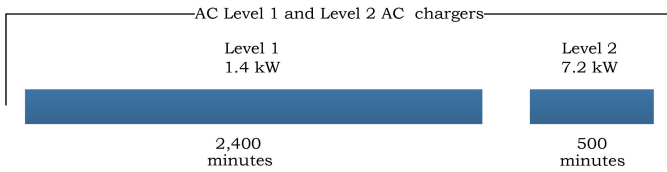


Fig. 9: AC charging power levels [17]

In the maritime sector there are ships that have AC propulsion systems. In this case, having an internal AC bus which can be connected to an AC onshore charger reduces the required conversion stages. This can be observed in the model from Fig. 10. The meaning of the symbols is the following: G is the back-up FF generator, T is the transformer, B is the battery, M is the motor and C represents converters. If the charging system were to provide DC instead of AC, at least one extra conversion stage would be required [18].

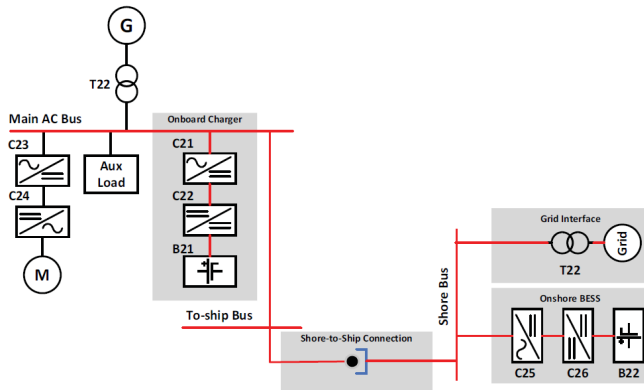


Fig. 10: AC charging for an electric ship with AC propulsion [18]

a) *Size*: The charger takes very little space outside of the vehicle, as it only provides a connection between it and the grid. Port adapters may be necessary, but do not require significantly more space. The AC-DC conversion and voltage levels management happens on board, which takes away from the usable space and mass.

b) *Efficiency*: The AC charging for vehicles is generally analysed in the context of LDV due to the power limitations that make charging HDV with AC not feasible. Paper [19] analyses the charging and discharging losses for in vehicles that use AC charging. Excluding the battery, the overall charging losses amount to 10.69% or 16.58%, depending on the current level used (40A and 10A, respectively). This results in efficiencies as low as 83.42% and as high as 89.31%.

In the maritime sector, a power loss analysis has been done in [18], where AC, DC, and inductive charging efficiencies have been calculated for ships with either DC or AC propulsion systems and different ratios of grid power and onshore battery power provided. In the case of AC propulsion ships, the highest charging efficiency is 85%.

c) *Sustainability*: AC charging has the inherent positive impact on sustainability goals of any EV charging technology,

as it is essential in the electrification and decarbonisation efforts. In the cases where less components and materials are required, such as the electric ship scenario described earlier, the matching of the load and supply power types improves the positive impact. The slower charging rates may improve EV battery lifetime and, although inconvenient, it may convince the user to use alternative methods of transport (such as bicycles or public transportation) more often. However, if the same aspect contributes to the delayed electrification of the transport sector, which is the case for HDAs, it consolidates unsustainable behaviours, such as using ICE-based vehicles.

d) *Economic Viability*: For LDV, AC chargers are the cheapest option, as most of the materials and related costs are shifted into the price of the car, where the on-board charger resides. In the maritime sector, AC charging is rarely the most efficient, which results in higher costs due to the power losses. Moreover, on-board charging is only suitable when a connection to a single phase grid is sufficient, which is not the case for this application. AC charging is not suitable for HDV and HDAs in general, because the provided power levels are too low; the slow charging results in longer inactive periods, which causes significant loss of profit for the transportation companies.

B. DC Charging

The other category of conductive charging, DC charging, is proving to be the solution for some of the issues of the AC counterpart. In this technology, the AC-DC conversion is moved outside of the vehicle, resulting in an off-board charger. For high power applications, state-of-the-art chargers have at least two stages: the front-end converts the three phase AC to DC while controlling the power factor, while the back-end controls the output voltage level and provides electrical isolation between the load and the grid [17]. The main characteristics and operational steps of such a system are described in the next section.

Due to the three phase connection and the fact that the of-board placements allows more space for power electronics and better heat dissipation, the voltage and power levels can reach much higher values than with AC, which is visible in Fig. 8. Getting a 60kWh battery to full charge can be done in very short periods of time, such as 10 minutes for a 350kW ultra fast (UF) DC charger, as presented in Fig. 11.

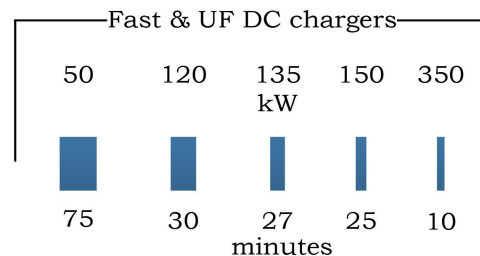


Fig. 11: DC charging power levels [17]

It is expected that DC fast charging will become the prevalent technology for HDA due to the aforementioned aspects. As HDV are a sector in which electrification is still at the beginning,

[14] summarised the essential specifications of some of the available DC fast chargers for the LDV sector. They can be observed in Table II.

TABLE II: DC chargers specifications [14]

Manufacturer	Output Power (kW)	Output Current (A)	Output DC Voltage Range (V)	Efficiency (%)
Blink DC Fast Charger	60	200	200–450	>90
eVGO DC Fast Charger	150	N/A	N/A	N/A
Chargepoint Express 250	62.5	156	200–1,000	96
Chargepoint Express plus	500	400	200–1,000	96
Greenlots	60	125	480	N/A
Bosch	25	65	200–500	94
Delta EV DC Quick Charger	50	125	50–500	94.6
BTC Power EVP-FC-50-001	50	100	50–500	>90
Schneider Electric	58	125	50–500	N/A
Tesla Super Charger	120	N/A	N/A	N/A
ABB Terra 54 HV Charger	50	125	200-920	95
ABB Terra HP	160	375-500	150-920	94

With a range of 25kW to 500kW, it is essential to establish the different scenarios in which an HDV would require charging. Slower chargers can be used overnight, when the speed demand is lower, which decreases the stresses on the battery circuitry and allows the use of cheaper chargers. Opportunity charging can be used in the off-times and breaks during a journey: the loading and unloading of trucks, the stops at bus stations of the electric buses. The highest power levels would be required from the ultra-fast chargers used "en-route": when there is not enough charge left to reach the next prolonged stop, an emergency charging-break must be taken and it should be as short as possible in order not to disrupt the transport schedule [4], [20]. A summary can be found in the form of Fig. 12.

TABLE III: Charging scenarios and the associated power levels [20]

Charger type	Nominal power output (kW DC)	Location	Estimated charging times
Overnight	50–150	Depot, public parking space	8 hours
Opportunity fast	150–350	Public charging station, depot, destination location	0.5 hours
Opportunity ultra-fast	750–3000	Public charging station, depot, destination location	0.5 hours

In the case of the maritime transport sector, DC charging allows better integration of the onshore batteries in the charging system, as well as allowing simpler connections with ships that have DC based propulsion. As the ships that transport large cargo or a great amount of people have very high power requirements, the local grids may not be able to support them.

MHDV Paradigm:

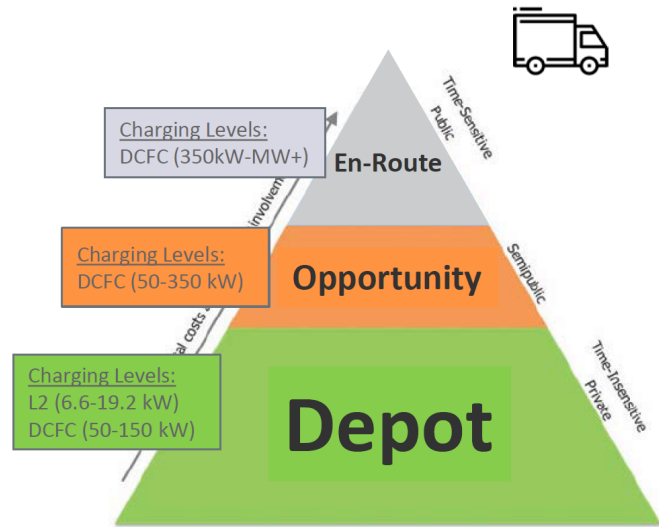


Fig. 12: HDV charging scenarios [4]

In such cases, onshore energy storage is necessary, as it provides the power that cannot be obtained from the grid. DC charging reduces the number of conversion stages that are needed in such a setup. The diagram in Fig. 13 shows this scenario; the symbols have the same meaning as described in AC charging.

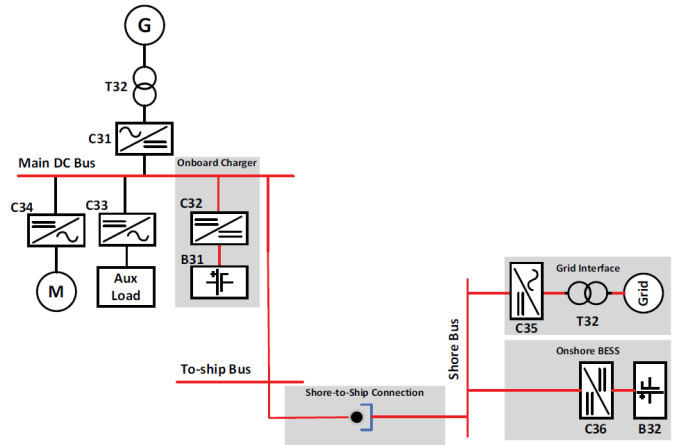


Fig. 13: DC charging for an electric ship with DC propulsion [18]

a) *Size*: As the DC fast chargers are off-board, there is more usable space and mass in the HDAs. However, this comes at cost of external space, as dedicated spots for the charging infrastructure, consisting mainly of charging stations, must be provided. This will take away from the garage space of depots, parking lots and might require a redesign of the roads with the most HDV traffic in order to accommodate emergency charging stations.

b) *Efficiency*: Compared to the data about AC charging, DC charging for EVs appears to be more efficient, as can be seen in Table II. All values recorded by [14] are above 90%, with

an average of approximately 94%. In the case of electric ships, DC charging is the most efficient technology for AC propulsion ships, as well as the best for DC propulsion ships when most of the power is provided by onshore batteries, according to [18]. The highest values are approximately 87% in both cases.

c) *Sustainability*: At the current stage, DC fast charging has the strongest potential to support the electrification of the HDAs, which directly supports the sustainability goals. Due to the large impact that the stations can have on the electrical and road infrastructure, as well as their long installation period, the integration of fast chargers must be thoroughly planned [20].

d) *Economic Viability*: Compared to AC chargers, DC chargers are more expensive in the LDV market, as the price must cover the off-board circuitry. In the case of HDAs, DC fast charging may be the technology that makes electric heavy duty transport financially viable. The current problems with battery prices, range anxiety, and extended periods of inactivity due to slow charging, issues that make FF-based transport more economically feasible, are improving. Upfront and maintenance prices for different DC charging levels can be observed in Table IV, based on the findings of [20]. The total upfront costs cover the hardware, software, planning, and installation. The yearly maintenance is calculated as 1.2% of the hardware and software costs. Chargers with 150kW and 1MW capabilities have the lowest cost per kW, whereas the 50kW charging is significantly more expensive. These findings show the high impact that the economy of scale can have on the economic viability of HDA charging.

TABLE IV: DC charging stations costs [20]

Public DC charger power	Total upfront costs	Total upfront costs per kW	Yearly operation and maintenance	Yearly operation and maintenance per kW
50 kW	€ 44,700	€ 894	€ 340	€ 6.80
150 kW	€ 91,700	€ 611	€ 840	€ 5.60
350 kW	€ 231,700	€ 662	€ 2,040	€ 5.83
1 MW	€ 615,800	€ 616	€ 5,300	€ 5.30

C. Inductive Charging

Wireless charging can involve different technologies, as presented in Fig. 14. In the context of HDA charging, inductive coupling is the feasible category, which is also called inductive power transfer (IPT). As it does not involve a direct connection, wireless charging is inherently isolated, which makes it safer both in the HDV and maritime sectors. In the latter, the mechanical isolation removes the risk of circuit corrosion, which is a great cause of concern for the wired technologies. A schematic depicting the connection through IPT between a DC propulsion electric ship, the grid, and the onshore batteries is shown in Fig. 15.

The functioning principle of IPT involves two coils and an AC signal: the signal energizes the primary coil, resulting in a varying magnetic field which induces an electromotive force in the secondary coil [8]. This is illustrated in Fig. 16. The efficiency of the power transfer is highly dependent on the

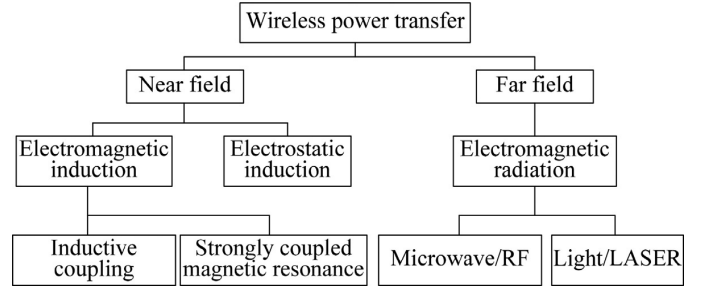


Fig. 14: Inductive charging technologies [8]

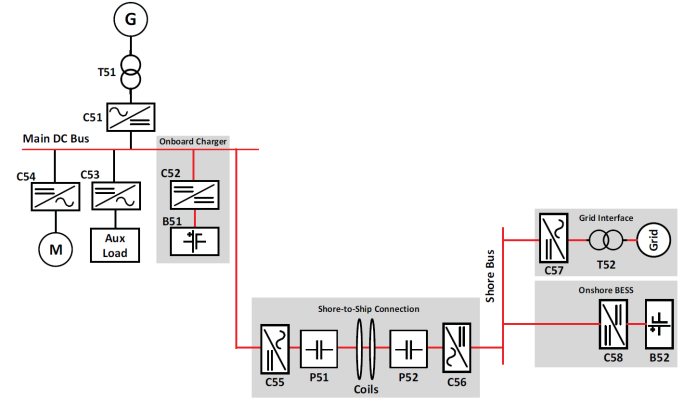


Fig. 15: Inductive charging for an electric ship with DC propulsion [18]

alignment of the two coils. Due to this reason, the placement of the two sides of the charger is particularly important and it complicates the layout of the charging stations and limits the design freedom of the HDA manufacturers. The movement of a berthed ship makes proper coil coupling harder and less efficient than making the connection through a cable.

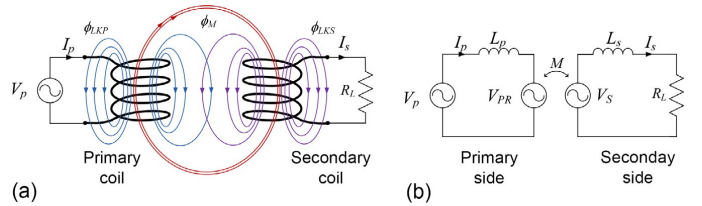


Fig. 16: IPT system model [8]

Outside of ideal and unrealistic coupling conditions, some of the magnetic flux produced by the current flow in the coils results in self-inductance. This inductance decreases the efficiency of the power transfer in a analogous way as reactive power does in a conductive charger. The issue of reactive power and the power factor in AC-DC converters is treated in the following section. In the case of IPT, the effect of the self-inductance can be reduced by including compensating capacitors in the circuit, as shown in Fig. 17 [8]. This circuit is similar to the DC-DC conversion stage that is analysed in the next section, with the significant difference that instead of the strongly coupled coils of the transformer, here the power

transfer is done through the loosely coupled coils of the two sides of the charger.

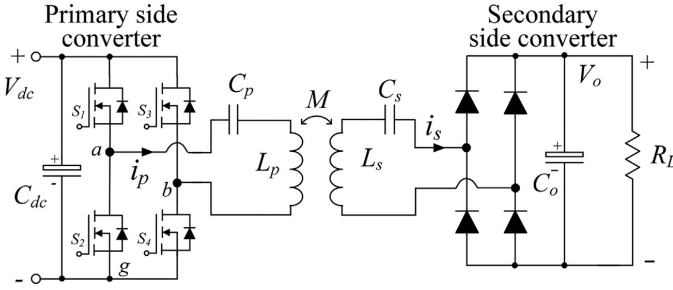


Fig. 17: IPT compensation circuit [8]

A summary of the findings of multiple research groups is provided by [14] and can be seen in Table V. the research is split between the two main charging scenarios for IPT: stationary and dynamic. In the first, the HDA does not move, as it is parked or docked in the dedicated spot next to the IPT station. The latter applies to HDVs, as it refers to them getting charged while they are moving, as the IPT is integrated in the roads on which the vehicles drive. It can be seen that the power capabilities are relatively low, especially when compared to DC charging.

TABLE V: IPT specifications [14]

Research Group	Output Power max (kW)	Distance (cm)	f_o (kHz)	Efficiency (end-end) (%)
Stationary Charging				
Oak Ridge National Laboratory	120	15	22	97
Mojo Mobility	10	20	80–90	92
Evatran Plugless	7.2	10	N/A	90
WiTricity	11	≤ 25	80–90	91–94
Momentum Dynamics	200 (Combined four coils and power supplies)	30	N/A	“Equal to conductive”
ETH Zurich	50	16	85	N/A
WAVE Inc	50	17.8	23.4	92
NYU and HEVO Power	25	21	85–88	91
Showa Aircraft Co	30	15	22	91
Dynamic Charging				
KAIST	22/27	20	100	97
Korea Railroad Research Institute*	818 (rail-type system)	5	60	82.7
INTIS	30	15	35	90

*Research on IPT for high speed trains conducted in 2015: [21]

a) *Size*: The volume and mass of the inductive charger are split between the charging station and the HDA. As mentioned before, the necessity of strengthening the coupling between the two sides imposes limitations on both ends. However, if wireless charging is integrated into the road network used by HDVs, it could provide enough charging that the necessity of opportunity super fast charging highly decreases. The range of the vehicles would increase dramatically [20]. Although not

yet feasible, they could drive without stopping to charge, as long as the roads used provide sufficient power throughout the journey.

b) *Efficiency*: As can be seen in Table V, the efficiency of IPT is similar to that of DC chargers. The main issue is represented by the strong dependence on the placement of the HDA regarding the charging station. For electric ships, the findings of [18] show that IPT is better than AC, but worse than DC in the context of charging ships with AC propulsion. The same holds true for ships with DC propulsion if most of the power comes from the onshore battery system instead of the grid. When the grid has a bigger weight in the calculation, IPT becomes the least efficient. However, the maximum efficiency values of IPT are approximately 85% for both AC and DC propulsion.

c) *Sustainability*: The main cause of concern about IPT in the context of sustainability is the very high electromagnetic interference (EMI) that it can cause. The air gap between the coils results in very high voltages and currents to be used in order to achieve proper functionality, which leads to significant EMI. One solution could be the implementation of polyphase AC into IPT, which should reduce the peak EM fields [14]. This is not only important for the protection of the electric equipment surrounding the charging areas (stations, electrified roads), but also for the people and animals in close vicinity, as the effects of those emissions on them are not yet clear [20].

d) *Economic Viability*: Due to the low power levels, stationary IPT is not a viable solution for manned HDVs, but it could accelerate the development of unmanned, fully automatic transport vehicles. In the maritime sector, IPT simplifies the connection between the ship and the grid, which results in a lesser need for specialised personnel, therefore decreasing costs.

Dynamic IPT is estimated to have very high costs due to the high impact it would have on the road infrastructure. An expected price of 1.2 million U.S. dollars per kilometre is mentioned in [20]. However, the inductive roads could supply energy to both HDVs and LDVs and reduce the number of fast DC charging stations needed along the way. Not only would range anxiety be highly reduced or even removed if the journey is planned properly, but the required on-board capacity could consequently decrease, which results in smaller prices for the vehicles.

IV. COMPARATIVE SUMMARY AND DISCUSSION

The clearest result of the previous analyses is that, although currently quite common for LDVs, AC charging is not a viable technology for the future, especially in HDAs. Having the location on-board greatly limits the expansion of power circuitry and the required thermal management, while also decreasing the carrying capacity of the vehicles and ships. Therefore, the focus should shift strictly to DC and inductive charging.

In terms of size, DC charging has the least impact on the design and carrying capacity of the HDA. The only requirement is that the charging port is placed in an accessible position on the vehicle. However, the charging stations must bear the

spacial concern: secured cabinets housing the converter will be visible and take away space from parking lots, pedestrian paths and depots or they can be placed underground, which comes with greater costs and less accessibility. Inductive charging splits the circuitry between the station and the vehicle. The charging pad does not have a large volume, so little internal space is required from the HDA, but a large flat surface is required for higher power transfer. The placement of the pad on the HDV must match the stationary pad, which can be integrated into depot walls, floors, and streets, which means that the pads must be either on the sides or on the bottom of the vehicle. In the case of electric ships, the pads should be installed on the walls of the berths and piers and on the sides of the vessel; otherwise, pads installed in the water, below the ship, or in the air, above it, require more complex installation and are restricting the size of the chargeable ship.

When the efficiencies are compared, both methods have similar values in the surveyed literature. DC charging appears to have more consistent ratings as they range from 90% to 94% for HDVs. Inductive technology varies between 82.7% (when the rail-type system is included in the analysis) or 90% up to 97%. The analysis on charging for electric ships reveals that DC charging is always more efficient by a few percentages. Moreover, alignment of the pads, the distance between them, and the materials that separate them have a great impact on the efficiency of inductive charging.

From the perspective of sustainability, both technologies require long term planning and large scale infrastructural redesign. While DC stations reduce the usable parking space, depot storage and pedestrian walkways, dynamic IPT involves partial or total overhaul of the roads with the most heavy traffic. The EMI produced by the inductive chargers is another cause of concern, as the effects on surrounding circuitry are negative without proper shielding and more research is needed on its influence on human and animal health .

Lastly, the economic viability of the two technologies greatly varies based on the application and perspective of the main cost bearer. As DC charging requires little conversion-related circuitry compared to IPT, the price of the HDAs that use it is expected to be lower, while the charger itself will be more expensive. Inductive charging splits the hardware-related costs more evenly. Moreover, the installation of DC stations above ground is fairly simple if the grid is already adapted for the large, localized power transfer, resulting in lower costs. Although the case for above ground pads is similar for IPT, the greatest potential of the technology is achieved by installing it in the roads, which allows dynamic charging. Such an infrastructure project would require more complex feasibility studies, planning, and partial or total traffic interruption or redirection during construction; its success would greatly depend on the amount of IPT-enabled EVs that will use those roads. This results in much higher costs and risks than DC charging.

Considering the evaluated aspects, a mixed charging infrastructure is proposed. IPT should be first implemented in the automation industry, where the movement paths and the exact

power requirements of the machinery is known. It can be extended to berths and piers as part of the cold ironing concept. Later, once it reaches higher levels of technical maturity, it can be used in large infrastructure projects, such as designated EV roads with dynamic charging. In the meantime and for the other uses, especially for HDVs, DC charging is recommended. High voltage and current power stations can be installed in the same or similar locations as the fuels stations of ICE vehicles, as well as next to emergency lanes and resting spots. Public and private parking for HDVs should also provide charging opportunities at medium power outputs. Depots and garages where the EVs originate from or spend longer periods of time at should install a large number of medium and low power stations.

V. HIGH POWER DC CHARGING SYSTEM

Considering the findings in the previous section, a more in depth analysis of DC charging becomes relevant in the context of heavy-duty vehicles. In order to reduce weight and to increase the usable space inside the vehicle, a grid side converter (GSC) can include all the modules required for charging. Due to the high power requirements of such vehicles, low voltage, single phase grid connections may be insufficient and even detrimental to the grid if it leads to unbalanced phase voltages. Therefore, a three phase low or even medium voltage connection is required. High capacity stationary power banks may be necessary, acting as buffers, in the case that a medium voltage connection cannot be realised or is still insufficient.

Based on the mentioned aspects, a DC charger would have to: allow connection with the low or medium voltage grid, efficiently convert AC to DC, adapt to the DC requirements of the load, as well as provide galvanic isolation between the load and the grid for safety reasons. A basic AC-DC converter for a single phase could be as simple as a single rectifier diode and a smoothing output capacitor, or a full bridge rectifier, as can be seen in Fig. 18. However, such simple circuits can have very high ripple voltages (unless they use unfeasibly large capacitors) and AC current cannot be controlled. This makes them incompatible with the adaptability and power efficiency requirements. Moreover, they either include no isolation or they implement it by placing a transformer between the grid and the bridge rectifier.

A. Galvanic Isolation Transformer Placement

As transformers require AC signals to function properly, placing them between the grid and the GSC is a simple solution. Besides not requiring any DC-AC conversion to function and allowing the entire converter to be electrically isolated, they can be used to step down the voltage to the desired level. However, classical transformers have the great disadvantage of being large and heavy when operating at low frequencies. [23], [24] show the relations between the transformer core areas and the functional parameters, which result in an inverse proportionality between volume and frequency, as shown in Eqs. (1) to (5). The meaning of the symbols is explained in Table VI.

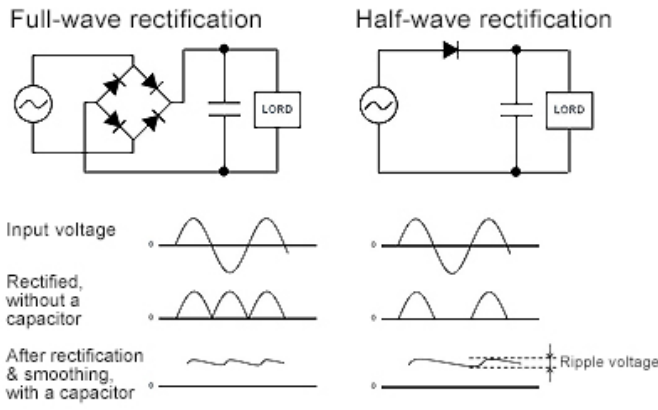


Fig. 18: Basic AC-DC converter circuits [22]

$$A_C = \frac{E_1}{\sqrt{2}\pi B_{max} f N_1} \quad (1)$$

$$A_W = \frac{2I_1 N_1}{k_W J_{rms}} \quad (2)$$

$$A_C A_W = \frac{\sqrt{2}S}{\pi k_W J_{rms} B_{max} f} \quad (3)$$

$$A_C A_W \propto L^4 \propto \frac{S}{f} \quad (4)$$

$$V \propto L^3 \propto \left(\frac{S}{f}\right)^{\frac{3}{4}} \quad (5)$$

TABLE VI: Meanings of the symbols used in the transformer equations

Symbol	Meaning
A_C	Core cross section area
A_W	Core window area
E_1	Voltage
I_1	Current
S	Rated power
k_W	Window utilisation factor
B_{max}	Amplitude of magnetic flux density
J_{rms}	Winding current density
f	Operating frequency
N_1	Number of turns on primary side
L	Length
V	Volume

For a given power rating, the volume-frequency and mass-frequency relations can be plotted, as shown in Figs. 19 and 20. From the first, it can be observed that an operating frequency of 1kHz results in approximate reduction of 90% in volume. Simultaneously, in the latter, the mass per power rating for ferrite cores with 99.5% efficiency drops from 30kg/kVA at 50Hz to 1kg/kVA at 1kHz.

A reduction in transformer core volume results in a lesser infrastructural impact, as the charging systems would require less space to be installed in. Moreover, the reduction in mass leads to smaller material and production costs, is more

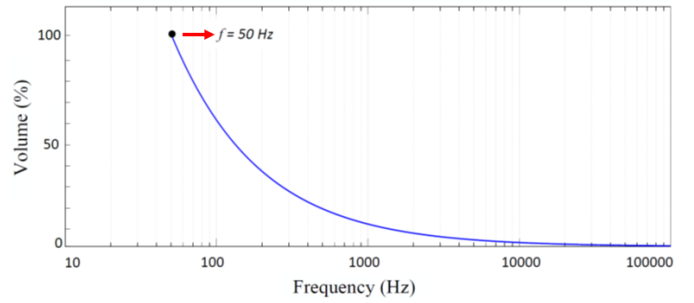


Fig. 19: Relation between transformer volume and operating frequency [23]

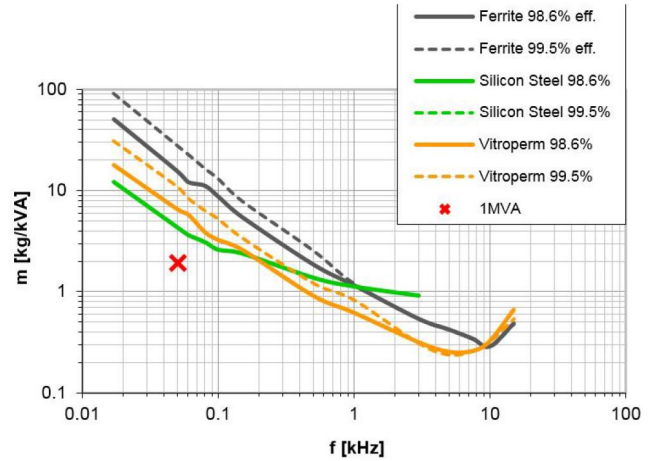


Fig. 20: Relation between transformer mass and operating frequency [24]

environmentally sustainable and allows the charger to become mobile if necessary. However, with all the added benefits of increasing the operating frequency of the isolating transformers, it is important to understand the limitations as well. As the volume of the transformer reduces, the surface area decreases as well, which complicates the thermal management: heatsinks might be required to increase the radiating area again in order to avoid overheating. In a smaller transformer, the conducting coils are placed closer together, which reduces the air gap that acts as an insulator. Under the high voltage conditions that such transformers operate in, the minimum size is limited by the required insulating air gap or by the existing insulating materials that can substitute it. Moreover, the high frequencies are above the ones used in the electrical grid and must either be derived from the grid frequency or generated separately.

Solid State Transformers (SST) are a technology that is capable of high power delivery while operating at medium frequencies (MF), as seen in Fig. 21, which makes them ideal in the context of GSCs. They are realised by a series connection of an inverter, an isolating transformer, and a rectifier: the DC is converted to MF AC, the voltage level is changed by the transformer's turn ratio and the resulting AC is converted back into DC. The operating frequency range makes them highly compact and energy dense, while the active switching in the

conversion stages allows the power routing to be more flexible, which is necessary for smart grids [25].

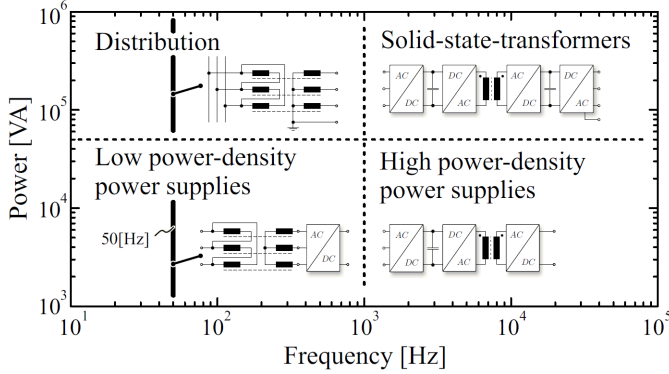


Fig. 21: The four main classes of electric transformers [25]

B. The Power Factor

From a power efficiency standpoint, the *power factor* is an essential aspect that needs to be considered. It is defined as the ratio between the real power and the apparent power and it is ideally unitary. This is the case for purely resistive loads connected to power supplies in the absence of noise or harmonic distortions. However, not only can the load have a complex impedance, but the transfer function of the circuit could be complex as well, due to inductive and capacitive elements. The reactive elements introduce a phase shift between the current and the voltage, which results in the reactive power being returned to the source when the two have opposite signs. If the current and voltage in the converter are purely sinusoidal, the power factor can be calculated using Eq. (6), where φ is the phase difference between the two [26].

$$PF_{phase} = \cos(\varphi) \quad (6)$$

However, if either the voltage or the current are not sinusoidal, harmonic distortion decreases the power factor as well. Assuming the grid can be modelled as an ideal voltage source, the current can be non-sinusoidal due to the non-linear elements in the circuit, like the diodes and the switches. Harmonic distortion decreases the power factor because only the fundamental frequency contributes to real power, while the harmonics result in reactive power. The relation between the real power and the reactive power can be expressed in terms of the phase difference and the *distortion factor* as seen in Eq. (7). The distortion factor is defined in Eq. (8), where THD (Total Harmonic Distortion) is calculated using Eq. (9) [26]. I_k is the current associated with each harmonic, with $k = 1$ corresponding to the fundamental frequency.

$$\begin{aligned} P_{IN_{real}} &= P_{IN_{apparent}} \cdot PF_{phase} \cdot PF_{THD} = \\ &= \sqrt{V_{IN_{RMS}} \cdot I_{IN_{RMS}}} \cdot \cos(\varphi) \cdot \cos(\theta) \end{aligned} \quad (7)$$

$$PF_{THD} = \cos(\theta) = \sqrt{\frac{1}{1 + THD^2}} \quad (8)$$

$$THD = \sqrt{\sum_{k=2}^{\infty} \frac{I_k^2}{I_1^2}} \quad (9)$$

For a high efficiency, the current must be "shaped" as to have a maximal power factor: it should be a sinusoidal signal with zero phase shift compared to the voltage. This can be realised through controlling the current, which is called *power factor correction (PFC)* in this case.

C. The Necessary Stages

Having considered the fundamental requirements of the charger, as well as the significance of the SST and PFC, a multistage implementation is chosen. It entails an AC-DC converter stage, representing the *front-end*, and a DC-DC stage as the *back-end*. The first one rectifies the three phase AC into an intermediary high DC voltage with ripples, while implementing a PFC module for increased efficiency. The latter reduces the ripples, controls and decreases the voltage to a medium level in order to match the load requirements and implements an SST to provide galvanic isolation. The output of the back-end passes through a decoupling capacitor to reduce any high frequency noise produced by the switching signals. A block diagram that depicts the two stages and the necessary control systems is presented in Fig. 22.

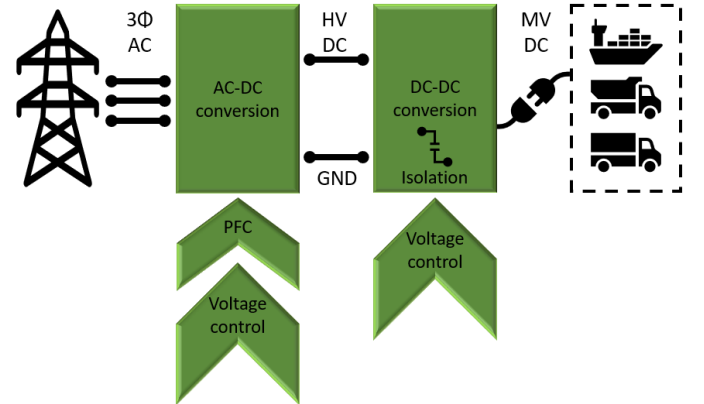


Fig. 22: DC charger block diagram: two conversion stages and related control systems

Each of the two stages is analysed in more detail in the following subsections.

D. AC-DC Stage

It is simpler to analyse a converter stage for a single phase, as the expansion to three phases is equivalent to adding some parts of the circuit (the input inductor and two switches) in parallel for each phase. There are multiple topologies that can be used to rectify the AC signal, such as: bridge, semi-bridgeless, AC switch and totem pole (TTPL) [27]. They can be observed in Fig. 23.

Although it requires the most complex control, the totem pole topology is chosen because it has the lowest amount of components while also having a high efficiency [27]. This is

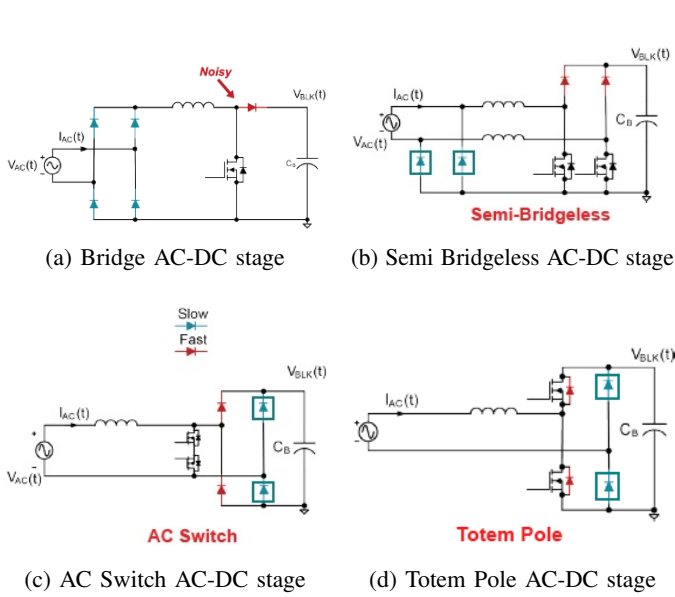


Fig. 23: Rectifier topologies

because the rectifying role of the bridge is combined with the control role of the transistors. For a single phase, the two diodes are sufficient as long as the converter is monodirectional. If a bidirectional converter is required, the diodes can be substituted with transistors, forming a second totem pole [28]. In the case of three phase power, the inductor and totem pole are replicated for each phase and connected in parallel. Therefore, no diodes are required and six transistors can be used instead. For example: the body diodes of the transistors in the second phase totem pole act as the rectifier diodes required by the first phase. With these considerations, the case of a dual totem pole (totem pole bridgeless) single phase converter is analysed.

1) **Functioning Principle:** If left uncontrolled, the current at the input of the rectifier will spike at every peak of the voltage amplitude, charging the output capacitor in a short amount of time. This can be mediated by shorting one of the supply branches to the ground, which stops the current delivery to the load and, if properly timed, charges the inductor. This step must be followed by reconnecting the supply and inductor to the load for a short enough time that current is delivered without spiking to the maximum value possible. In this way, the current signal required for power delivery can be shaped into an arbitrary periodic signal. For the reasons mentioned in the previous subsections, a sinusoid with no phase shift is preferred.

The control signals for the transistors are PWM-based and two control states can be defined for each voltage polarity (or current flow direction). The current paths associated with the four possible states are shown in Figs. 24 and 25. It is essential that the transistors on the same totem pole are never on at the same time in order to avoid short circuiting the load.

AC Voltage Positive, State 1: S1 is on and S2 is off, while S3 is off and S4 is on. This forces the current to flow from and

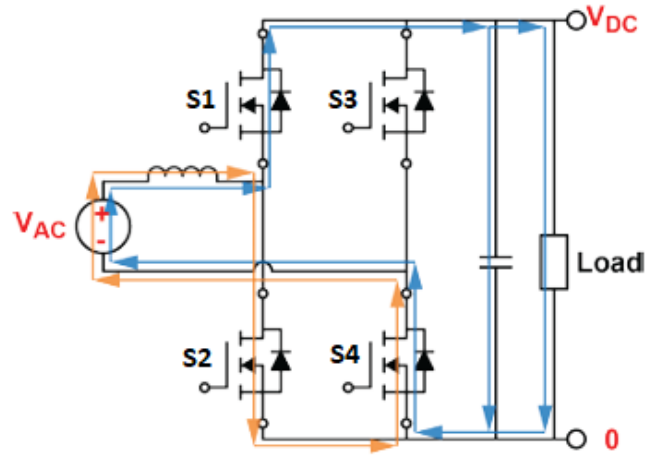


Fig. 24: Positive AC current path for state 1 (blue) and 2 (orange) [28]

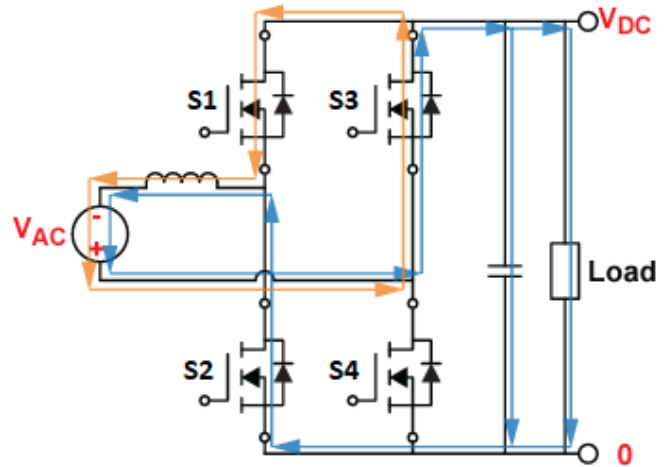


Fig. 25: Negative AC current path for state 1 (blue) and 2 (orange) [28]

source and inductor through the smoothing capacitor, charging it, and the load. Power is therefore delivered. The current flows back to the source through the body diode of S4.

AC Voltage Positive, State 2: S2 is on and S1 is off. The current flows to ground and through S4 back to the source. S3 and S4 could both be turned off, as the current would simply flow through the body diode of S4. However, turning S4 on is preferred because it would simplify the control logic (always having one of the driving signals in the totem pole be the inverse of the other) and it would remove the voltage drop caused by the diode. No power is delivered from source to load, but the inductor is being charged and the capacitor maintains a stable voltage over the load.

AC Voltage Negative, State 1: is similar to state 1 when the AC voltage is positive, but the current flow through the capacitor and load is in the opposite direction. S3 is on, S4 is off, while S1 must be off to prevent current to flow directly

back to the inductor and source, thus forcing it through the load. S2 could be off and current would still flow through the body diode, but, due to the previously mentioned reasons, it is preferred to be on. The control signals are the inverse of the ones used in the AC Voltage positive stage 1 and the same as in stage 2.

AC Voltage Negative, State 2: is similar to AC Voltage Positive state 2, but now the loop is realised on the high rail (positive V_{DC}) instead of the ground rail. The current flow is in the opposite direction compared to the mentioned state, but the same principle applies: the inductor gets charged, no power is transmitted from source to load and the capacitor maintains the output voltage.

2) **Parameter Design:** The simulated AC-DC stage is part of a GSC connected to a low voltage, three phase grid. This results in the input voltage to be 230V (phase to neutral), at 50 Hz in order to simulate the electrical grid used in Europe. The output of the stage is $V_{bus} = 850V$ DC, which represents the intermediary (bus) level between the stages. The load is selected as $R_{load} = 45\Omega$, which draws approximately $P_{out} = 16,056kW$ according to Eq. (10). The simulation analyses the ideal scenario in which there are no losses due to switching or internal resistances and the component values are calculated with a unitary PF in mind.

$$P_{out} = \frac{V_{bus}^2}{R_{load}} \quad (10)$$

The most important components for the functionality of the converter are the switches. Based on the typical voltage and current ratings for high power supplies, as well as the requirement of efficient control (both simple and non-lossy), a choice must be made between the Metal-Oxide-Semiconductor Field-Effect-Transistor (MOSFET) and the Insulated Gate Bipolar Transistor (IGBT). The main difference, application-wise, is that the MOSFETs are better suited for high frequency switching (100 kHz and higher) and low current density conduction, while the opposite is true for IGBTs. Moreover, IGBTs have comparatively reduced EMI and lower on-state and switching losses, as well as requiring smaller heatsinks due to their thermal efficiency [29]. Therefore, the choice is made to use IGBT switches, with a driving frequency $f_{switch} = 10kHz$.

The output capacitor has the role of smoothing out the high frequency ripples caused by the switching, as well as compensating for any imbalance in the phase line [30]. The allowed maximum ripple is $V_{ripple} = 0.4V$ peak. The capacitance is determined using Eq. (11), where P_{out} is the output power. Therefore, a suitable value would be $C_{out} = 800\mu F$.

$$C_{out} \geq \frac{P_{out}}{2\pi \cdot f_{switch} \cdot V_{ripple}} \approx 752\mu F \quad (11)$$

The inductors are chosen based on the maximum input current allowed. In an ideal circuit, the input power is equal with the output power, so a maximum ripple current of 10% can be calculated using Eq. (12), with V_m being the peak line to neutral voltage. The relation between the ripple current and

the inductor value is explained in [30]. Therefore, Eq. (13) can be used, where M is the modulation index calculated as Eq. (14). The actual value chosen is $L = 3mH$.

$$I_{ripple} = 0.01 \cdot \frac{P_{out}}{V_m} \approx 4.28A \quad (12)$$

$$L = \frac{V_{bus}}{6 \cdot I_{ripple} \cdot f_{switch}} \cdot M \approx 2.53mH \quad (13)$$

$$0 < M = \frac{\sqrt{3} \cdot V_m}{V_{bus}} < 1 \quad (14)$$

3) **Voltage Control:** The output voltage is controlled using a simple feedback loop. The output is continuously monitored and its value is subtracted from the reference, giving an error signal. The error signal is passed through a Proportional Integral (PI) controller with gains $K_P = 0.0001$ and $K_I = 1$. The result is passed further in the current control loop.

4) **Current Control:** The PFC can be implemented using different methods, either passive (strictly based on circuit design, no control loops) or active. The latter has many categories and subcategories, such as continuous, discontinuous, and critical conduction mode (CCM, DCM, CrCM) [31]. The categorisation of some of the PFC techniques can be observed in Fig. 26.

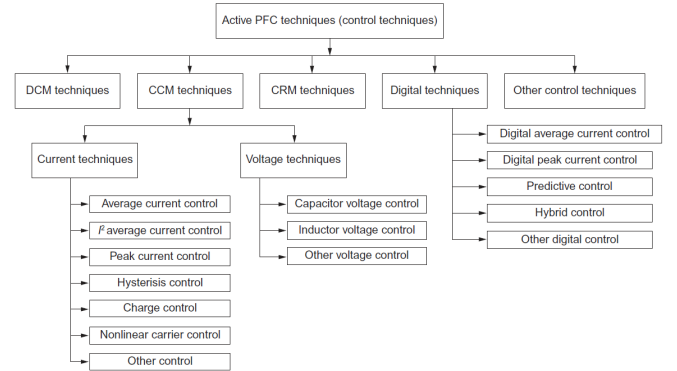


Fig. 26: PFC techniques grouping [31]

In an initial attempt, the current is controlled using the *hysteresis* technique. It involves two control references, called "current commands" [31]: one that is slightly higher and one slightly lower than the ideal reference level. They represent the *high command* and *low command* and the difference between the two forms the *hysteresis band*. The band and the associated signals can be visualized in Fig. 27, where i_{hcmd} , i_{cmd} , and βi_1 are the high and low commands, and the measured input current, respectively. As long as the measured signal is inside the hysteresis band, no control action is taken. Once it goes beyond the high or low commands, the transistors are switched to either decrease or increase it respectively. The width of the band can be arbitrarily set, and it must be narrowed in order to decrease the input ripple current. However, in doing so, the switching frequency is increased [31].

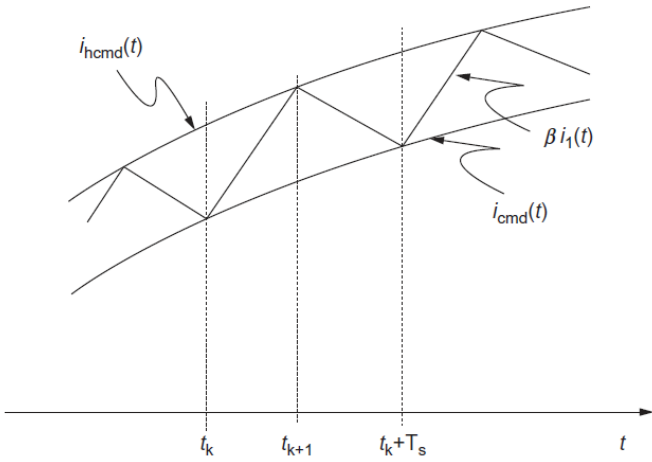


Fig. 27: Visualisation of the hysteresis band [31]

The hysteresis technique allows for direct control over the input current shape and the ripple amplitude, but it indirectly sets the switching frequency. Moreover, the frequency changes in a range depending on the part of the sinusoid's period in which the switching is happening at the moment (higher frequency close to the zero crossing, lower frequency at the peaks). This makes the design of the electromagnetic interference (EMI) filter and the reduction of THD more complicated [31]. Therefore, another technique is preferred, similar to constant frequency peak current control. As the name suggests, the command is represented by the reference signal; the measured signal is increased (by turning on the relevant switches) to reach it and, once it does, the switches are turned off. This can be done using a constant switching frequency. In this case, a higher frequency allows for smaller adjustments, which lowers the current ripple. This technique directly controls the switching frequency, but indirectly controls the shape of the signal.

A disadvantage of these techniques, especially of the latter, is the high control effort (high switching frequency) that is required for satisfactory results. This leads to higher switching losses, which decreases efficiency and, thus, reducing the added benefit of implementing PFC. Following a variable reference point requires more effort than a constant one. If a DC signal were to be followed, instead of a sinusoidal AC one, the system would have a better efficiency. In that scope, the *direct quadrature zero* (D-Q-Z or D-Q) transformation can be used [32].

An in-depth explanation about the D-Q transform is outside the scope of this paper, therefore only a brief one is presented; interested readers are referred to [33] for more details. The D-Q transform is based on the Clarke and Park transformations and it allows the mapping of the three rotating vectors (A, B, and C) associated with the line phases from a static three dimensional space to two static vectors (D and Q) in a rotating two-dimensional plane. A spatial representation of the Park transformation is shown in Fig. 28 in order to provide an

intuitive graphical understanding of the D-Q transform. The 3 phase AC signals corresponding to the line currents can be mapped to two DC signals and no information is lost as long as the phase angles have been measured as well. Those are necessary for reversing the transformation.

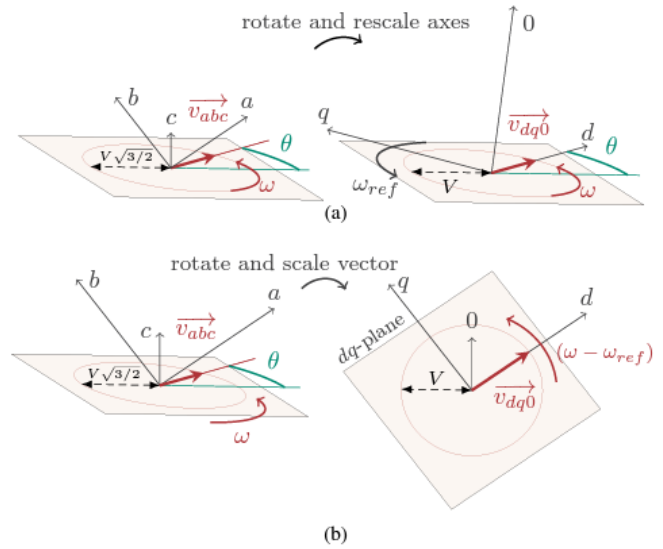


Fig. 28: Standard Park transformation: axes transformation (a), vector transformation (b) [33]

To understand the role of the transformation in the PFC controller, the control loop is analysed. Both the measured input currents and the references (scaled version of the three input AC voltages) are transformed to D-Q coordinates. A phase lock loop (PLL) module measures the phases of the line voltages before the transformation. The newly obtained DC signals are processed as follows: the D coordinate measured signal is subtracted from the corresponding D coordinate reference and the resulting error is sent through a PI controller with gains $K_P = 0.1$ and $K_I = 0.01$. The same is done for the two Q coordinate signals. The outputs of the PI controllers are transformed back to ABC values using the phases measured by the PLL. Each of the three AC values is used to modulate a triangle wave carrier to produce a PWM driving signal.

5) **Simulation Results:** The output of the front-end stage reaches the required value very quickly: it takes 0.5s to reach 845.207V and 1s to reach 849.449V. These voltages are 99.44% and 99.94% of the targeted 850V. The fast response and stability of the converter can be seen in Fig. 29.

The input voltage and current are shown in Figs. 30 and 31, where their amplitudes are normalized. The first figure focuses on the transient response of all three phases and demonstrates the speed of the PFC controller: the current (green) follows the same shape and phase of the voltage (red) in less than 0.5s. The initial peak in current is determined by the large voltage difference between the initial output and the target voltage. A close-up of the synchronised input current and voltage is included in the second figure. The measured THD for all phases is approximately 0.0147.

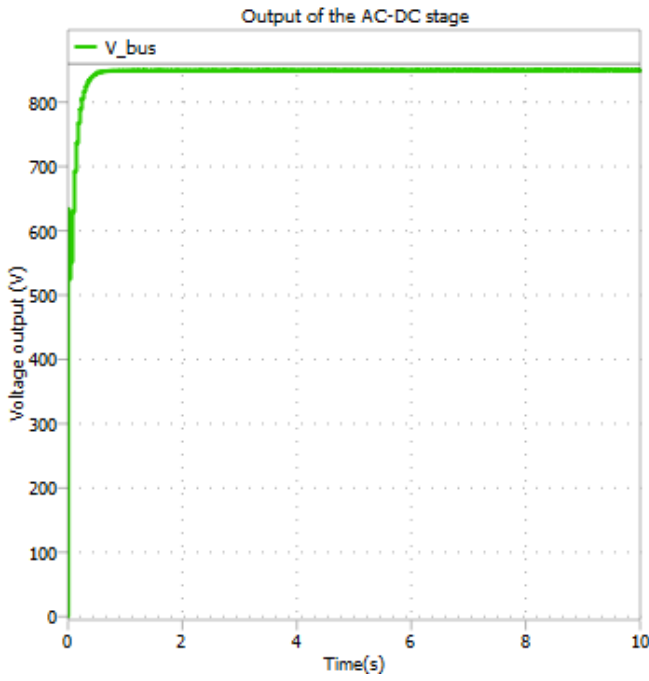


Fig. 29: Output of the TTPL PFC 3 phase converter

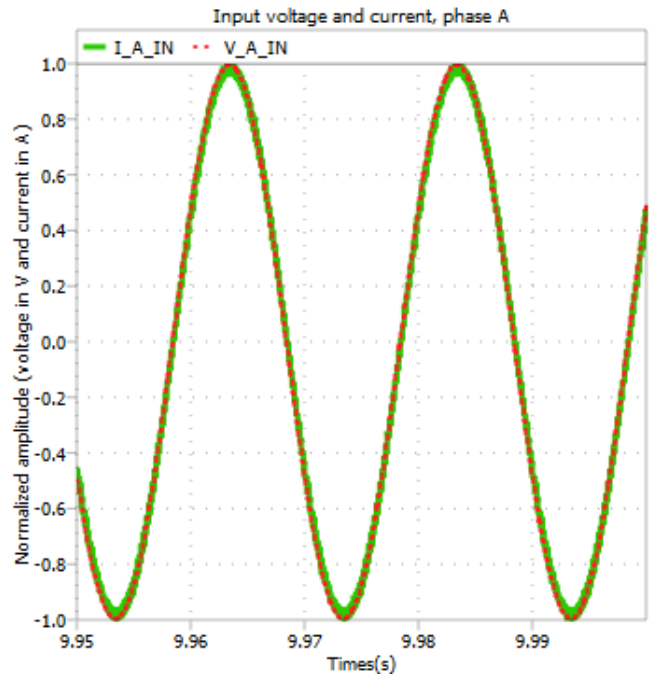


Fig. 31: Input voltage (red, 400V/unit) and current (green, 54A/unit) during stable period

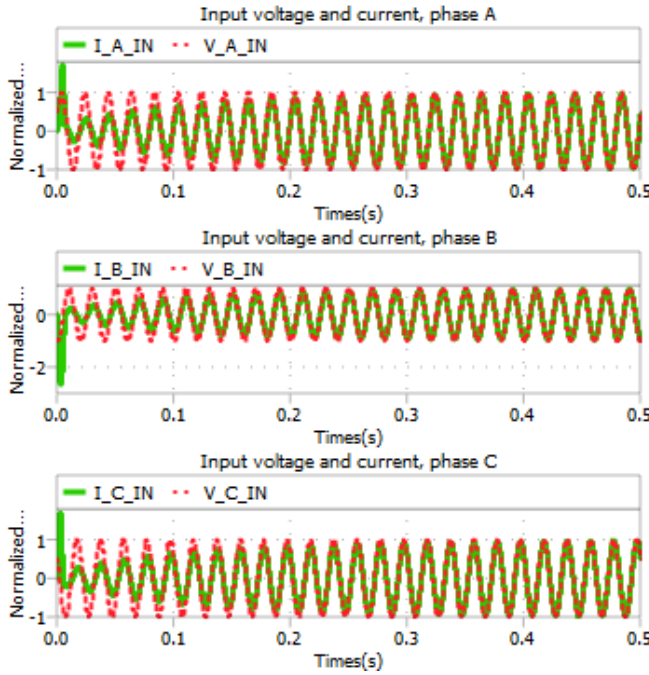


Fig. 30: Input voltage (red, 400V/unit) and current (green, 54A/unit) during transient period

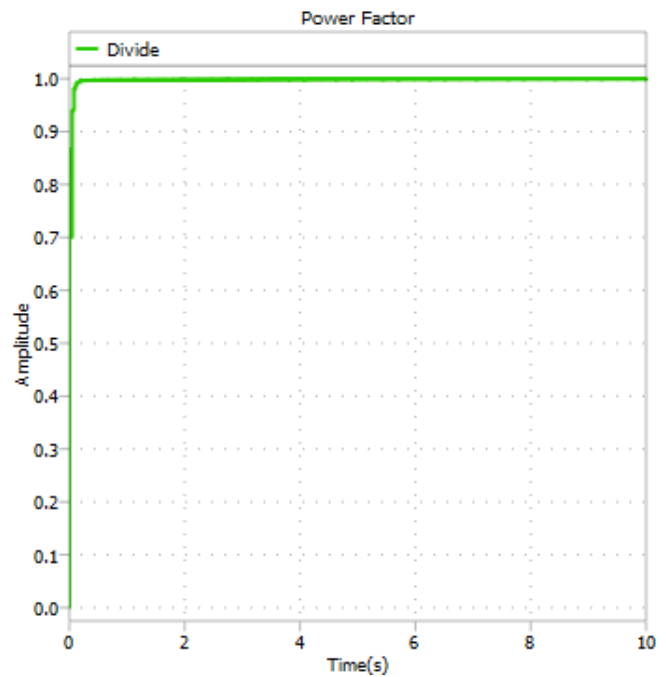


Fig. 32: Power Factor of the TTPL PFC 3 phase converter

A PF measurement circuit model designed by [34] is included in the simulation and its output is shown in Fig. 32. In just 0.5s, the power factor is 0.997, which confirms the quick response of the PFC controller. At the end of the 10s simulation, the PF is almost ideal: 0.999.

E. Phase Shifted Full Bridge Rectifier DC-DC Stage

The previous conversion stage outputs a controlled DC voltage, usually much higher than its input RMS value. The charging bus of the heavy-duty vehicles might require varying nominal values, which can exceed the output limitations of the AC-DC conversion. Moreover, the high voltages are a

concern for the user safety. For these reasons, a second stage is implemented, which fulfils the DC-DC conversion and isolation requirements of the charger.

The DC-DC conversion can be realised by a multitude of circuits, of which 8 are considered to be distinctive enough to represent independent topologies: boost, buck-boost, buck, flyback, forward, push-pull, half bridge, and full bridge [35]. However, only the latter three are suitable for high power applications, as they are double ended. The terminology is related to the operation of the transformer and is described in the following paragraphs.

The transformer: is an essential element in the functionality of the converter and it has a significant impact on the overall efficiency, as its saturation leads to significant losses. The flow of current in the primary winding of the transformer generates a magnetizing force (H), which creates a magnetic flux (B) in the magnetic core [36]. The idealized relation between the two can be graphically described by the B-H curve, as seen in Fig. 33. The flux density changes almost linearly with the magnetizing force in a certain range limited by the saturation points. Once the flux density reaches these thresholds, it will not continue to significantly increase or decrease even is the force becomes stronger. The functionality of the converter requires the operation of the transformers in the non-saturated range, where the relation between the flux and the force is mostly linear.

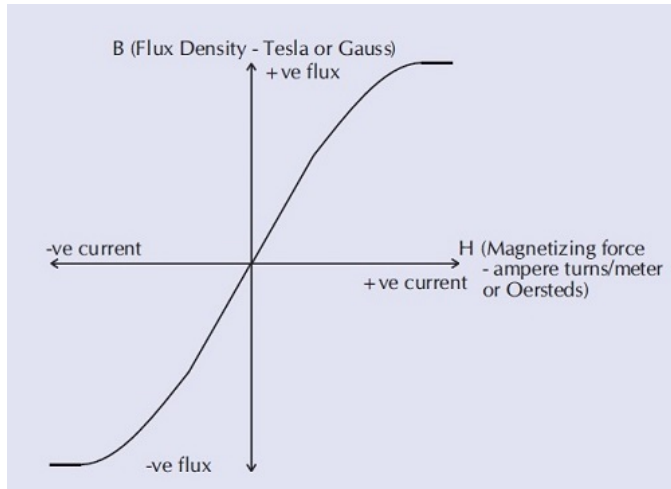


Fig. 33: Idealized B-H curve [36]

However, realistic material have the property of *remanence*, which describes the fact that the magnetization of a magnetic material does not change instantly and it does not reduce to zero even when the force H is null. Therefore, the B-H curve follows the shape seen in Fig. 34, which is named the hysteresis loop of the transformer [36].

In such a plot, the four quadrants can be defined based on the sign of B and H. The operation of the transformer in the conversion cycles happens either in only one of the quadrants (Q1 or Q3) or in both. A single ended converter makes use only of the first quadrant, while a double ended one

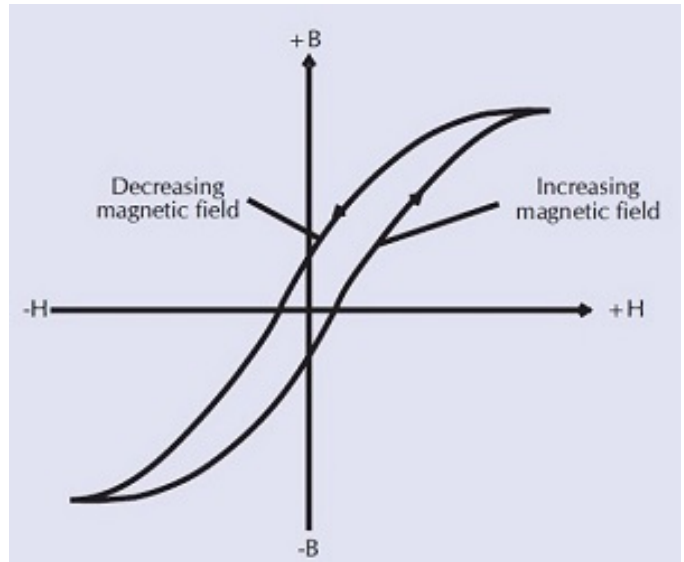


Fig. 34: Hysteresis loop of the transformer[36]

uses both quadrants, making better use of the linear range of the transformer [35]. The graphical representation of the two operation principles can be observed in Figs. 35 and 36:

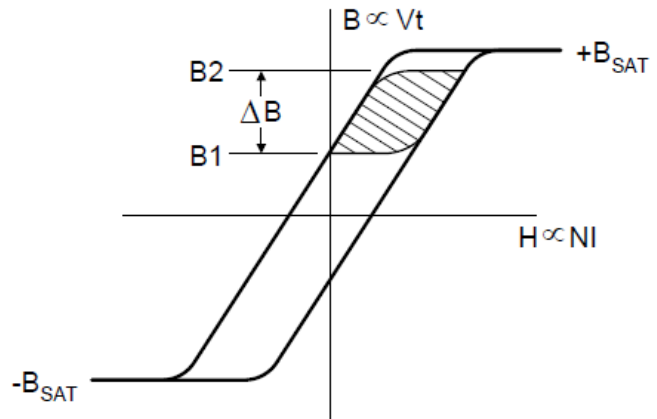


Fig. 35: Hysteresis loop of single ended converters[35]

The choice is left between the three topologies: the push-pull, the half bridge, and the full bridge. The first converter requires centre-tapping the primary transformer winding, which forces the switches to withstand double the input voltage value. The half bridge avoids this issue by using two capacitors to form a rail splitter, allowing a voltage drop over each switch no higher than the input. However, the input ripple currents can lead to overheating of the capacitors if they are not chosen correctly, which can heavily damage the circuit. The full bridge solves the issues of both topologies by using four switching transistors, having the higher component count and more complex driver signals as the only disadvantages [37]. A circuit diagram of the full bridge DC-DC converter can be observed in Fig. 37.

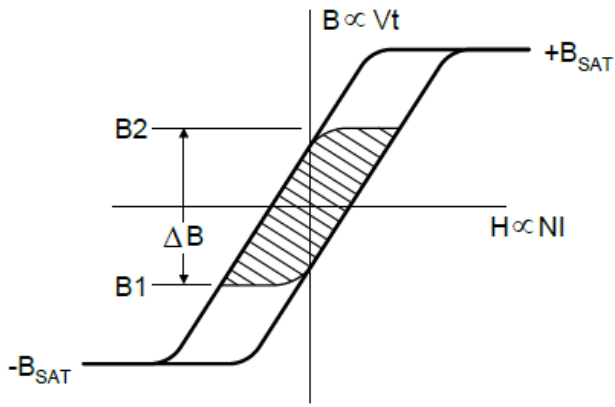


Fig. 36: Hysteresis loop of double ended converters[35]

1) **Functioning Principle:** The input is connected through a decoupling capacitor. This component allows the flow of high frequency ripple currents to the ground, improving the quality of the DC output of the previous stage. The four switches required by the full bridge are implemented through insulated gate bipolar transistors (IGBTs). They are controlled by gate drivers as to produce an intermediary AC signal, which energizes the primary side of the isolating transformer. The latter changes the voltage level depending on the ratio of coil turns between the primary and secondary sides. Four diodes form the rectifier that converts the intermediary AC signal back into DC. The latter is passed through an LC filter, at the output of which the external load is connected.

The full bridge converter diagram can be observed in Fig. 37. As [38] focuses on the noise analysis of this circuit, the internal diode of the IGBTs and their parasitic capacitance is depicted in the diagram. Similarly, the parasitic capacitance of the transformer is included in the diagrams in Fig. 38. However, a thorough analysis that covers the parasitic effects is out of the scope of this section and they have not been included in the simulation.

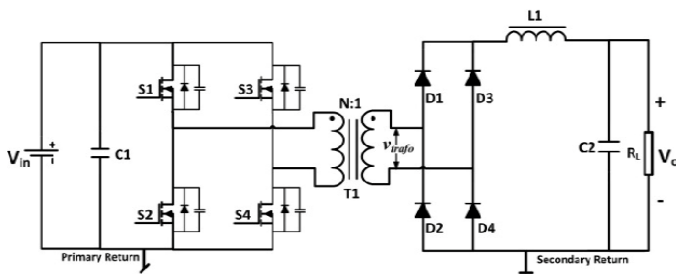


Fig. 37: PSFB circuit diagram [38]

Another aspect that is outside the scope of the simulation, but which is nonetheless important for realistic PSFB applications, is the addition of a snubber circuit. The transition periods the switches can generate voltage and current ringing at the output of the converter. The voltage spikes can reach double the voltage over the secondary side of the transformer. Although soft switching can decrease these effects, usually a snubber

circuit is needed. Such circuits have different topologies as well and can either be passive or active. Usually, active snubbers are more energy efficient, but are more complex because they require specific driving signal to function [39]. Another method in which the efficiency of the PSFB can be increased is the implementation of MOSFETs instead of diodes on the secondary side. They can be controlled to obtain synchronous rectification, which decreases the conduction losses during low voltage - high current output periods [40].

In the classical full bridge, the switches S1 and S4 are driven by the same Pulse Width Modulation (PWM) signal, while S2 and S3 are controlled by the inverted signal. This results into *hard switching*, when the change in the on/off state of the switch happens while both the current and voltage are non-zero, which leads to switching noise and losses. In order to improve overall efficiency, *soft switching* is the preferred method, which entails the change of the state when either the current or the voltage are zero [41]. Soft switching can be realised in the full bridge by introducing a phase shift in the driving signals of S3 and S4 compared to the ones controlling S1 and S2. The resulting circuit is called the Phase Shifted Full Bridge (PSFB) converter.

The functionality of the PSFB can be described in each stage of the operational cycle, similarly to how it was analysed in [38]. The current path in the four stages can be observed in Fig. 38. It is worth noting that in state 1 the current flows through the switches and diodes highlighted in red, while in state 3 it flows through the ones that are greyed out.

In state 1: S1 and S4 are on and allow the current to flow from the input, through the decoupling capacitor and through the primary side of the transformer. Power is delivered to the secondary side and it flows through diodes D1 and D4. Energy is stored in the output inductor L1. At the end, S4 turns off, its capacitance starts to charge and S3's capacitance discharges.

In state 2: the charging and discharging of the capacitances of switches S4 and S3 is followed by the flow of magnetizing current on the primary side. It is a consequence of the energy stored in the inductance of the transformer. The current flows through S1 and the body diode of S3, reducing the voltage drop over the latter to zero. This zero voltage allows S3 to be soft switched on in this state. This mechanism is employed with all switches that turn on in the following states. With S1 and S3 turned on, the voltage over the transformer is zero as well, therefore no power is delivered. However, the inductor L1 keeps the current flowing through the four diodes, the output capacitor, and the load. In this state, the currents flow without the involvement of the voltage sources and are considered to be *freewheeling*. Therefore, the state is categorised as freewheeling, as opposed to power delivering.

In state 3: S1 is turned off and S2 turns on through soft switching. With S2 and S3 on, current flows in the reverse direction through the primary side of the transformer compared to state 1. This leads to diodes D2 and D3 to be used on the secondary side. Power is delivered to the load.

In state 4: S3 is off and S4 is soft switched on. The magnetizing current starts freewheeling on the primary side

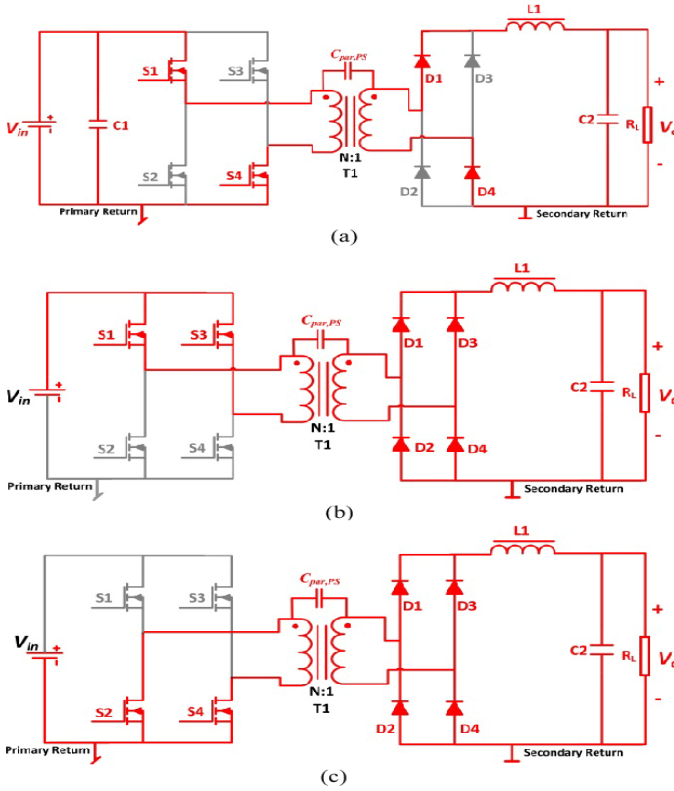


Fig. 38: PSFB current flow path in state 1 and 3 (a), state 2 (b), and state 4 (c) [38]

through S2 and S4. No power is delivered, but current flows through all the diodes on the secondary side due to the energy stored in L1, similarly to state 2. As S2 turns off, the operational cycle ends and a new one begins in state 1 when S1 is soft switched on.

2) **Element Parameter Design:** The simulated DC-DC converter represents the back-end of the GSC, resulting in its input voltage to be the output of the previous stage, V_{bus} . The intended output is $V_{PSFB} = 400V_{DC}$. The load is set as $R_{PSFB} = 10\Omega$, resulting from Eq. (15) in an output power of $P_{PSFB} = 16kW$.

$$P_{PSFB} = \frac{V_{PSFB}^2}{R_{PSFB}} \quad (15)$$

The reasoning for the choice of switches is the same one as for the TTPL PFC stage. The choice for the output inductor and capacitor is similarly based on the allowed ripple voltage and current. Therefore, the PSFB uses IGBT switches and has the output filter elements with $L_{PSFB} = 0.00001H$ and $C_{PSFB} = 0.08F$. The input decoupling capacitor has the same value as the output capacitor of the front-end stage, as it has the same role in the GSC. The transformer ratio is chosen based on the transfer function from [35], written in Eq. (16). The maximum duty cycle D that stops a short circuit of the positive and negative rails of the input is 50%, therefore the middle of the operable range, $D=25\%$, is chosen as to also

allow boosting if necessary. The transformer ratio, $n_s : n_p$, is 16:17.

$$\frac{V_{PSFB}}{V_{bus}} = 2 \cdot \frac{n_s}{n_p} \cdot D \quad (16)$$

3) **Voltage Control:** In a stable situation, lacking any disturbances, the output of the converter can be found easily by using the transfer function. In such a scenario, only a basic open loop control must be realised in order to generate the four states of the operational cycle. Therefore, a PWM generator with the preferred frequency and duty cycle is implemented, as well as a phase shift of 90° for the switches S3 and S4.

However, a more realistic scenario includes the existence of disturbances. These can be noise or instability in the input (errors from the previous stage) or changes in the load. In order to maintain a stable voltage output, a feedback control loop is implemented. The output is constantly monitored and its value is subtracted from a reference value. The result is fed into a PI controller with gains $K_P = 0.01$ and $K_I = 0.01$. The output of the PI controller is compared with the PWM signal: if the PI output is high, the monitored DC signal is lower than the reference and the duty cycle must be increased. If the opposite is true, the DC signal is too high and the duty cycle must be decreased.

4) **Simulation Results:** The output voltage and power of the PSFB reach the target values of 400V, and 16kW respectively, in less than 0.1s, as can be seen in Fig. 39.

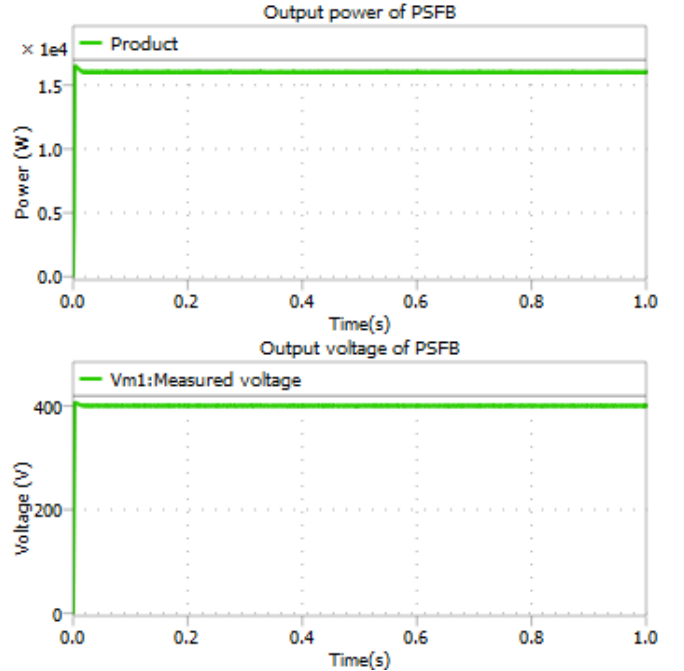


Fig. 39: PSFB power and voltage output

F. Combining the Stages

After the two stages have been designed and tested separately, they have been merged into a single GSC circuit. The output of

the AC-DC stage directly connects to the input of the DC-DC stage, replacing the voltage source and the input decoupling capacitor. Each stage is controlled individually, as described in the previous subsections.

The output voltage and power of the GSC are shown in Fig. 40. The values reach the references after approximately 4s. At 0.57s the voltage is 419.59V. It reaches 404.63V at 2s and finally, at 4s it is equal to 400.63V. The value of the power has a higher overshoot but stabilizes at a similar time as the voltage. The intermediary bus voltage follows the same trend in the transient and stable periods, which can be seen in Fig. 41.

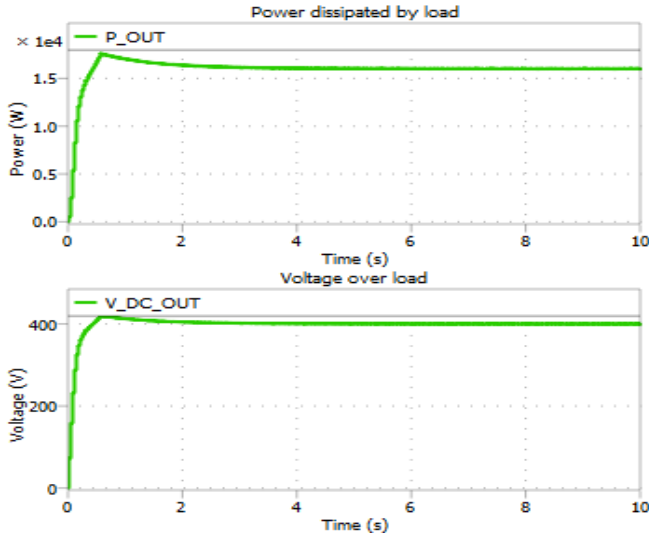


Fig. 40: GSC output power and voltage

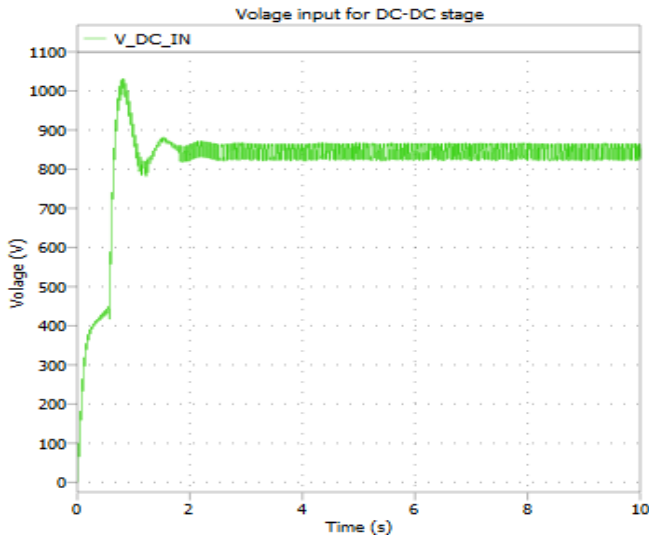


Fig. 41: GSC bus voltage

The response of the PFC controller can be observed in Figs. 42 and 43. The first figure shows the transient response of all three phases, which start having a synchronised current and voltage in the period 0.2s - 0.4s. The second zooms in the

finals 0.05s of the simulation, where the two values are clearly matched and the THD is 0.0147. The power factor goes from 0.990 at 0.5s to 0.999 at the end of the simulation.

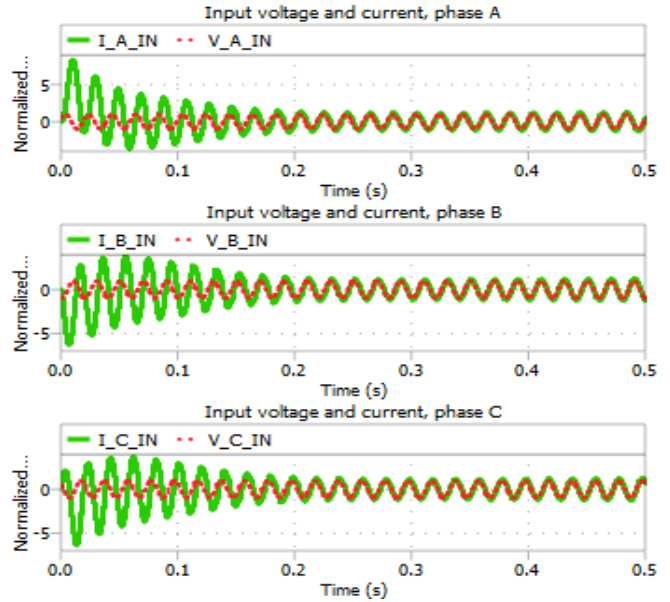


Fig. 42: GSC input voltage (red, 400V/unit) and current (green, 54A/unit) during transient period

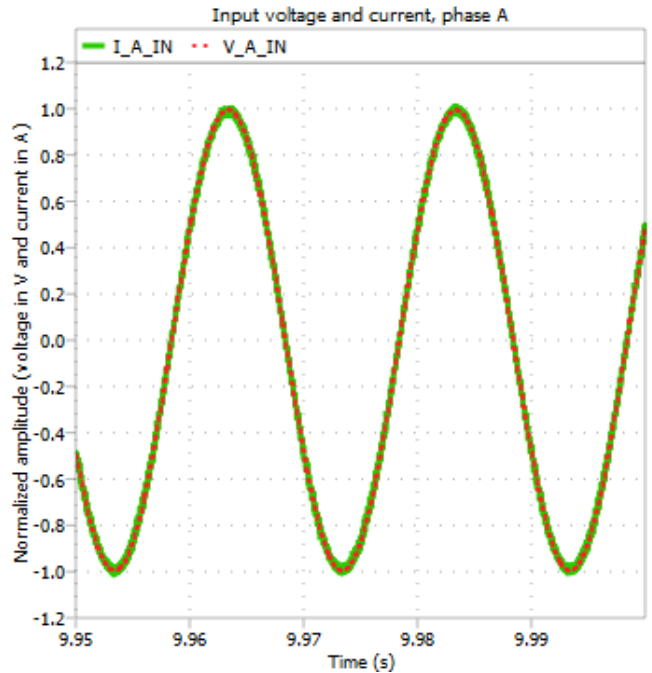


Fig. 43: GSC input voltage (red, 400V/unit) and current (green, 54A/unit) during stable period

VI. DISCUSSION ON DC CHARGING

The simulation of the two stages, both individually and together, has the main purpose of verifying the concepts behind

the topologies and their control schemes. The stable outputs at the intended levels confirm that the functional principles have been properly applied. The quick response time without large overshoots or unintended oscillations suggest that the factors of the PI controllers have been correctly chosen and that the transformation to and back from D-Q coordinates is successful.

The circuits contain only the ideal versions of the strictly necessary components, without parasitic effects or voltage and current breakdown limitations, as they are outside the scope of this study. Therefore, the results show idealized behaviour, with very short transient periods followed by fully stable states. The exclusion of parasitic capacitances in the transistors and the leakage inductance of the transformer results in fewer resonant frequencies, which improves the THD and decreases the amplitude of the ripples.

Moreover, the simplified circuits allows the controllers to correct the values faster, which explains the quick stabilization. This is emphasized by contrasting the transient period length of any of the two individual stages with the one of the GSC. The individual testing involved constant voltage sources and constant, purely resistive, loads. This resulted in stability being reached in less than a second for both the bridgeless TTPL and the PSFB stages. When the two are combined, the back-end appears as a variable load to the front-end, while the front-end is seen as a variable voltage input to the back-end. Each of the controllers is therefore indirectly influenced by the others, which results in an almost quadrupled length for the transient period. For example, the voltage controller of the PSFB allows more current to flow during the power stages in order to reach the target output as quickly as possible; the higher power drain at the end of the TTPL circuit can be seen as a quickly decreasing load resistor. Therefore, not only is a high current drawn from the grid in order to reach the intended 850V bus voltage, but even more is required in order to compensate for the apparently decreasing load of the front-end stage. This can be observed in Fig. 41, where the voltage quickly increases in two portions, with a "break" in between, where it slows down. The break happens immediately after the 400V mark is reached, when the back-end stage stops boosting the voltage and starts reducing it instead.

The lack of an overall power efficiency measurement is another consequence of the idealized model. As no power is dissipated through parasitic resistances or thermal losses of transistors (they have instant switching and no thermal model), the power factor remains the only relevant element of efficiency.

The values of the components, especially of the resistive load have been chosen for demonstration purposes. In the context of the idealized models, all values could have been scaled up or down: the chosen output power is 16kW, but it could have been 16MW if the load were 1000 times smaller. However, scaling can be done by increasing the voltage as well. For a constant resistance, power scales up quadratically with the voltage; a factor of 1000 for power results in an approximate factor of 31.62 for the voltage. Therefore, the bus voltage in such a circuit could reach up to at least 26.88kV. The values in ranges of tens of kilovolts are problematic for realistic

power transistors and diodes, which have limited breakdown voltages. As the required charging power keeps increasing, the high voltage stresses are likely to become the main limiting factor. In this scenario, multilevel approaches could be the solution: the circuit of one of the stages is formed by multiple converter cells with output connected in series. The voltage drop over each cell is equal and only a fraction of the total voltage. Therefore, the transistors and diodes can be operated in their safe voltage range while the complete system uses much higher values. If the circuit design is modular enough, future-ready charging stations can be constructed with enough room to later install more levels for each stage, which enables easy upgrading, upscaling and more redundancy in the design.

VII. CONCLUSION

The transport sector has a high impact on the overall global GHG emissions, but it also holds a great potential for decarbonization. Two of its subsectors, the heavy-duty vehicles and maritime, are undergoing an accelerated electrification process which can only be continued with the support of high power charging technologies. Due to the multitude of option, selecting the most viable candidates is essential for the planning of the charging infrastructure.

This paper has briefly presented the context in which the HDAs are being developed and in which their limitations and requirements are defined. It has expanded upon the three main categories of charging systems: AC, DC, and inductive, out of which the latter two were considered as feasible solutions. From the perspectives of size, efficiency, sustainability, and economic viability, DC charging was chosen as being the best fit for most applications in the near future, while IPT could complement it in the automation industry and high EV traffic roads.

A DC charging system was analysed and simulated in order to showcase its functional principles. Two conversions stages, AC-DC for the front-end and DC-DC for the back-end, were separately described. A high efficiency topology, the TTPL PFC was selected for the front-end. Its current control involved D-Q transformations for quicker operations which resulted in an almost ideal power factor, while the voltage control was realized by a simple and efficient PI controller which maintained the stability of the output. The back-end implemented a PSFB topology, which can handle high voltage stress and power, while having minimal switching losses due to its soft switching capabilities. It also had the function of galvanic isolation, as it formed a SST in the DC-DC stage: the use of high switching frequencies allows smaller magnetic cores to be used in the transformer. Although a single level system was presented, it was recommended to extend the analysis to multilevel converters so that the matured power electronics could safely share the stresses caused by the high voltage required by future chargers.

VIII. LIMITATIONS AND FUTURE RESEARCH

This paper presents a general overview of the current state of charging technologies for electric heavy duty applications

and showcases the main aspects and operational principles of DC charging as part of a case study. However, given more time, the scope could further be expanded to include a comprehensive literature survey and analysis on state-of-the-art charging systems, as well as an in-depth description of multiple specific converter topologies. Therefore, from the perspective of this paper representing just the basis of a more detailed study, the following topics are suggested as relevant follow-up research goals.

A. *Extended Literature Survey*

The comparative analysis can be expanded upon by increasing the number of reviewed sources. The EV technology and the transport sector are developing at an accelerated pace and represent topics of interest for contemporary research. Multiple sources that were used in this paper have been published in the current or past year, with the others being very recent as well. The speed at which electric HDA technology is progressing requires periodic evaluations of newly released research results. Moreover, developments in adjacent fields, such as automation, data processing, manufacturing, semiconductor physics, could be followed as part of a trend analysis in the power electronics and EV sector.

B. *Multilevel Implementation*

The current case study analyses a charging system with two conversion stages, both being single level circuits. As mentioned in the discussion, it is expected that the charging voltage for future HDA batteries will increase. Considering the voltage breakdown limitations of current semiconductors, a solution for higher power and voltage systems can be multilevel design. Cascaded H-bridge cells keep their switches under low and equal stresses while their outputs are connected in series and add up to a much higher total voltage. This allows the system overall to use medium and high voltages without having to wait for the development of new power semiconductors, at the cost of higher component count and more complex driving signals and control. Moreover, the multiple levels also allow a better PWM reconstruction of sinusoidal signals, which decreases the harmonic distortion. In such systems, the filters have more lax specifications or can be entirely removed, which decreases the number components used and the related costs.

C. *Parasitics Modelling and Realistic Switching*

As stated in the case study, the simulated circuits used idealised models of the components. The inclusion of main parasitics, such as semiconductor capacitances and resistances, and leakage transformer inductance, results in a more in-depth analysis of the system's behaviour. Such simulations can be used in the design of either a realistic charging system, that can be built and tested, or a controller for such a system. Moreover, the main argument supporting the use of PSFB topology is the soft switching of the transistors, which decreases losses. Although the simulation implements phase shifted driving signals, the effects of soft switching are impossible to analyse due to the lack of capacitances in the transistor model.

Furthermore, the switches have an instantaneous transition from on to off state and vice-versa, while transition times should also be taken into account if switching losses are included in the analysis.

D. *Thermal Losses Modelling*

The PLECS software is used for the design and simulation of the circuit because its library includes not only electrical and control models, but also thermal ones. Elements such as heat sinks, thermal resistors and capacitors, and thermal junctions can be used to extend the otherwise electric analysis to the thermal domain. Moreover, the semiconductor components allow the inclusion of specific thermal models, which can be taken directly from the manufacturer's datasheets. A modelling and calculating the thermal losses can help in the design of a realisable charging system and adds another point of comparison between the different technologies and implementations.

E. *Overall Losses and Efficiency calculation*

The simulation of the DC charging system can be used as a verification tool for the overall efficiency and the main sources of energy losses. After including parasitic elements, realistic switching behaviour and thermal models, different topologies and configurations can be compared in terms of efficiency as well. Moreover, the performance of the simulated circuits should be compared to that of already built state-of-the-art chargers as a mean to identify possible improvements.

F. *Circuit Analysis of AC and Inductive Charging*

Following the results of the literature survey, realistic circuit simulations of the other two charging technologies can be used to extend the comparison. This approach could reveal both fundamental differences as well as common points in the chargers. For example, the similitude between the PSFB and the compensation circuit for IPT suggests that driver signal patterns could be simultaneously developed for both if the same operational principles apply. Given the proposed approach of using a mixed charging infrastructure, it is important to use the knowledge from more mature technologies to accelerate the development of the newer ones.

ACKNOWLEDGEMENTS

No part of my student experience would have been possible without the continuous support from my parents and I am grateful for all the opportunities that stemmed from their countless efforts. During these three years, I was able to transform many of those opportunities into good, unforgettable memories, which made me appreciate all of the friends, colleagues, and teachers that I met along the way and who helped me enjoy my journey. In the context of my work, I would like to specifically thank Alexandre Lopez and Ali Sakr for proofreading and constructively criticizing parts of my thesis. Finally, I thank my supervisors for their guidance throughout this exciting and, at times, confusing last module.

REFERENCES

- [1] European Commission, *Questions and answers on the commission strategy for reducing heavy-duty vehicles' (hdvs) fuel consumption and co2 emissions*, Last accessed 23 June 2023, 2014. [Online]. Available: https://ec.europa.eu/commission/presscorner/detail/en/MEMO_14_366.
- [2] U.S Department of Energy, *Vehicle weight classes & categories*, Last accessed 23 June 2023. [Online]. Available: <https://afdc.energy.gov/data/10380>.
- [3] CarQuest Professionals, *Heavy duty vehicle type & weight class*, Last accessed 23 June 2023. [Online]. Available: <http://www.carquestprofessionals.com/filters/pdf/Heavy-Duty%5C%20Vehicle%5C%20Type%5C%20%5C&%5C%20Weight%5C%20Class.pdf>.
- [4] M. Muratori and B. Borlaug, *Perspectives on charging medium-and heavy-duty electric vehicles*, Last accessed 25 June 2023, 2021. [Online]. Available: <https://www.nrel.gov/docs/fy22osti/81656.pdf>.
- [5] International Council on Clean Transportation, *Heavy vehicles*, Last accessed 23 June 2023. [Online]. Available: <https://theicct.org/sector/heavy-vehicles/>.
- [6] International Council on Clean Transportation, *Maritime shipping*, Last accessed 23 June 2023. [Online]. Available: <https://theicct.org/sector/maritime-shipping/>.
- [7] International Energy Agency, *Global ev outlook 2023 catching up with climate ambitions*, Last accessed 25 June 2023. [Online]. Available: <https://iea.blob.core.windows.net/assets/dac14d2-eabc-498a-8263-9f97fd5dc327/GEVO2023.pdf>.
- [8] S. Arora, A. T. Abkenar, S. G. Jayasinghe, and K. Tammi, *Heavy-Duty Electric Vehicles: From Concept to Reality*. Butterworth-Heinemann, 2021, Last accessed 25 June 2023, ISBN: 978-0-12-818126-3. DOI: <https://doi.org/10.1016/C2018-0-02433-0>.
- [9] Drive to Zero, *Zeti data explorer*, Last accessed 25 June 2023. [Online]. Available: <https://globaldrivetozero.org/tools/zeti-data-explorer/>.
- [10] O. MacDonnell, Y. Qiu, X. Wang, S. Song, C. Dobbe-laere, and P. Cristiano Façanha, *Zero-emission truck and bus market update*, Last accessed 25 June 2023. [Online]. Available: https://globaldrivetozero.org/site/wp-content/uploads/2022/10/ZE_TruckBus_update.pdf.
- [11] Electric Vehicle Database, *Useable battery capacity of full electric vehicles*, Last accessed 13 June 2023. [Online]. Available: <https://ev-database.org/cheatsheet/useable-battery-capacity-electric-car>.
- [12] American Battery Solutions, *Construction, agricultural & mining*, Last accessed 13 June 2023. [Online]. Available: <https://www.americanbatterysolutions.com/applications/construction-agriculture-mining>.
- [13] P. Vaughan, *What's driving evs to higher battery voltages?* Last accessed 13 June 2023. [Online]. Available: <https://www.electronicdesign.com/markets/automotive/article/21249715/power-integrations-whats-driving-evs-to-higher-battery-voltages>.
- [14] D. Smith, B. Ozpineci, R. L. Graves, *et al.*, “Medium- and heavy-duty vehicle electrification: An assessment of technology and knowledge gaps,” Feb. 2020, Last accessed 25 June 2023. DOI: 10.2172/1615213. [Online]. Available: <https://www.osti.gov/biblio/1615213>.
- [15] S. Qazi, P. Venugopal, G. Rietveld, *et al.*, “Powering maritime: Challenges and prospects in ship electrification,” *IEEE Electrification Magazine*, Jun. 2023.
- [16] DC Velocity Staff, *Cold-ironing to have electrifying effect on california port*, Last accessed 30 June 2023, 2010. [Online]. Available: <https://www.dcvelocity.com/articles/24861-cold-ironing-to-have-electrifying-effect-on-california-port>.
- [17] A. Ahmad, Z. Qin, T. Wijekoon, and P. Bauer, “An overview on medium voltage grid integration of ultra-fast charging stations: Current status and future trends,” *IEEE Open Journal of the Industrial Electronics Society*, vol. 3, pp. 420–447, 2022, Last accessed 25 June 2023. DOI: 10.1109/OJIES.2022.3179743.
- [18] S. Karimi, M. Zadeh, and J. A. Suul, “Evaluation of energy transfer efficiency for shore-to-ship fast charging systems,” in *2020 IEEE 29th International Symposium on Industrial Electronics (ISIE)*, 2020, pp. 1271–1277. DOI: 10.1109/ISIE45063.2020.9152219.
- [19] E. Apostolaki-Iosifidou, P. Codani, and W. Kempton, “Measurement of power loss during electric vehicle charging and discharging,” *Energy*, vol. 127, pp. 730–742, 2017, Last accessed 26 June 2023, ISSN: 0360-5442. DOI: <https://doi.org/10.1016/j.energy.2017.03.015>. [Online]. Available: <https://www.sciencedirect.com/science/article/pii/S0360544217303730>.
- [20] M. R. Bernard, A. Tankou, H. Cui, and P.-L. Ragon, *Charging solutions for battery-electric trucks*, Last accessed 26 June 2023, 2022. [Online]. Available: <https://theicct.org/wp-content/uploads/2022/12/charging-infrastructure-trucks-zeva-dec22.pdf>.
- [21] J. H. Kim, B.-S. Lee, J.-H. Lee, *et al.*, “Development of 1-mw inductive power transfer system for a high-speed train,” *IEEE Transactions on Industrial Electronics*, vol. 62, no. 10, pp. 6242–6250, 2015, Last accessed 27 June 2023. DOI: 10.1109/TIE.2015.2417122.
- [22] TechWeb, *Ac-dc basics*, Last accessed 17 June 2023. [Online]. Available: <https://techweb.rohm.com/product/power-ic/acdc/acdc-basic/12619/>.
- [23] S. Qazi, *Transformer size: Why move to medium frequency?* Last accessed 23 June 2023.
- [24] J. W. Kolar and J. E. Huber, *Fundamentals and application oriented evaluation of solid state transformer concepts*.
- [25] G. Ortiz, M. Leibl, J. W. Kolar, and O. Apeldoorn, “Medium frequency transformers for solid-state-transformer applications — design and experimental verification,” in *2013 IEEE 10th International Conference on Power Electronics and Drive Systems (PEDS)*,

- Last accessed 23 June 2023, 2013, pp. 1285–1290. DOI: 10.1109/PEDS.2013.6527217.
- [26] ON Semiconductors, *Power factor correction (pfc) handbook: Choosing the right power factor controller solution*, Last accessed 17 June 2023. [Online]. Available: <https://www.onsemi.com/pub/Collateral/HBD853-D.PDF>.
- [27] B. McDonald and B. Lough, *Power factor correction (pfc) circuit basics*, Last accessed 18 June 2023. [Online]. Available: <https://www.ti.com/seclit/ml/slup390/slup390.pdf>.
- [28] S.-Y. Yu, X. Gong, G. Wang, and M. Bhardwaj, *Designing a high-power bidirectional ac/dc power supply using sic fets*, Last accessed 18 June 2023. [Online]. Available: <https://www.ti.com/seclit/ml/slup393/slup393.pdf>.
- [29] Bourns, “White paper: IGBT vs. MOSFET – determining the most efficient power switching solution,” Tech. Rep., 2022, Last accessed 21 June 2023, p. 11. [Online]. Available: https://www.bourns.com/docs/technical-documents/technical-library/igbt/bourns_igbt_vs_mosfet_determining_efficient_power_switching_solution_white_paper.pdf.
- [30] H. Hafezinasab, *Investigation of solutions for universal input 208 V-480 V three-phase ac/dc power factor corrected converters with 400 V DC output*, Last accessed 21 June 2023. [Online]. Available: <https://open.library.ubc.ca/media/stream/pdf/24/1.0392472/4>.
- [31] A. Kouzou, “Power factor correction circuits,” in *Power Electronics Handbook*, M. H. Rashid, Ed., 4th ed., Last accessed 20 June 2023, Butterworth-Heinemann, 2018, ch. 16, pp. 529–569, ISBN: 978-0-12-811407-0. DOI: <https://doi.org/10.1016/C2016-0-00847-1>.
- [32] G.-J. Chiou, J.-Y. Chen, T.-C. Chen, and B.-X. Chen, *Application of d-q axis transformation control strategy for three-phase ac/dc converter*, Last accessed 20 June 2023. [Online]. Available: <https://ieeexplore.ieee.org/document/6527137>.
- [33] C. J. O’Rourke, M. M. Qasim, M. R. Overlin, and J. L. K. Jr., *A geometric interpretation of reference frames and transformations: Dq0, Clarke and Park*, Last accessed 20 June 2023. [Online]. Available: <https://dspace.mit.edu/handle/1721.1/123557>.
- [34] B. Lieblick, *Power factor*, (Message and file posted to website address) Last accessed 28 June 2023, 2021. [Online]. Available: <https://forum.plexim.com/7724/power-factor>.
- [35] S. Mappus, *Power converter topology trends*, Last accessed 13 June 2023. [Online]. Available: https://www.psmas.com/sites/default/files/uploads/files/10%20PSMA%20PTR%202014_10_02%20Power%20Converter%20Topology%20Trends%20Mappus%20Fairchild.pdf.
- [36] Voltech, *The basics of transformers*, Last accessed 14 June 2023. [Online]. Available: <https://www.voltech.com/support/technical-articles/transformer-basics/>.
- [37] S. Roberts, *Dc/dc book of knowledge*, Last accessed 14 June 2023. [Online]. Available: https://recom-power.com/en/support/technical-resources/book-of-knowledge/book-of-knowledge.html?8-2.-layout-main-layout_body-layout_body-main-dataView-viewContainer-rows-2-item-dataView-viewContainer-rows-4-item-dataView-gridContainer-rows-5-cols-2-item-dataView-viewContainer-rows-1-item-card-imageLink.
- [38] I. A. Makda and M. Nymand, “Common-mode noise analysis, modeling and filter design for a phase-shifted full-bridge forward converter,” in *2015 IEEE 11th International Conference on Power Electronics and Drive Systems*, 2015, pp. 1100–1105. DOI: 10.1109/PEDS.2015.7203521.
- [39] I. Ferencz, D. Petreus, and T. Pătăraș, “Comparative study of three snubber circuits for a phase-shift converter,” in *2020 International Symposium on Power Electronics, Electrical Drives, Automation and Motion (SPEEDAM)*, Last accessed 30 June 2023, 2020, pp. 763–768. DOI: 10.1109/SPEEDAM48782.2020.9161962.
- [40] S. Lee and J.-W. Park, “A new control for synchronous rectifier of phase-shifted full-bridge converter to improve efficiency in light-load condition,” *IEEE Transactions on Industry Applications*, vol. 57, no. 4, pp. 3822–3831, 2021, Last accessed 30 June 2023. DOI: 10.1109/TIA.2021.3071106.
- [41] Toshiba, *Please explain hard switching and soft switching using IGBTs*, Last accessed 15 June 2023. [Online]. Available: https://toshiba.semicon-storage.com/ap-en/semiconductor/knowledge/faq/mosfet_igbt/igbt-012.html.